Morphometry and Density Analysis of the Fifth Metacarpal

by

Amrita Unnikumaran

A thesis submitted in partial fulfillment
of the requirements for the degree of
Master of Science in Biomedical Engineering
Department of Medical Engineering
College of Engineering
University of South Florida

Co-Major Professor: William E. Lee III, Ph.D.
Co-Major Professor: Peter Simon, Ph.D.
Robert Frisina, Ph.D.
Sergio Gutierrez, Ph.D.

Date of Approval:
October 25, 2019

Keywords: Bone Geometry, Bone Density, Computerized Tomography Scan Study, Sexual Dimorphism

Dedication

I dedicate this work to my family for their immense support and encouragement.

Acknowledgments

I would like to express my sincere gratitude to my mentor Dr. Peter Simon and Dr. William Lee for their guidance and motivation which helped me succeed.

I very grateful to Dr. Robert Frisina and Dr. Sergio Gutirezz for their valuable time and suggestions which kept me motivated. I would also like to extend my gratitude to University of South Florida and Foundation for Orthopaedic Research and Education for giving me the opportunity to learn and experience high quality research.

Table of Contents

List of Tables

List of Figures

Abstract

The fifth metacarpal bone fracture is a common type of fracture among the young male population. With the increasing demand for early recovery from such fractures with surgical reduction, the medical manufacturers and clinicians are interested in designing a better intramedullary device for fixation. This study is an attempt to investigate the dimensional parameters of the fifth metacarpal bone and its intramedullary canal, using 3D CT scan images of cadaveric hands. The algorithm used for measurement applies principal component analysis on the subject bone, to control the information loss and normalize the spatial position of the subject. This analysis provides a range of measurements for bone-length, the diameter of scribed circles for both the whole bone model and intramedullary canal, as well as the density distribution of the cortical bone. The results indicated that there is a statistically significant relationship between the height of specimen donors with respect to the length of bone, and the diameter of the scribed circles for their intramedullary canal ($p < 0.1$). There is also a statistically significant correlation between the average density of the cortical bone with respect to the weight and BMI of the donor specimen ($p \leq 0.05$). However, the correlation was less evident in the female population than compared to that of the male population. These measurements evidence enough variability within the demography, suggesting a requirement for a wider range of devices to cater to a diverse patient population.

Chapter 1: Introduction

1.1 Study Motivation

Metacarpal fracture is a common type of fracture which contributes to 40% of all hand fractures [1]. A study conducted between 2002 to 2006 highlighted an incident rate of 29.7 per 100,000 person-years for hand fractures in the USA, wherein 13.6 per 100,000 person-years was the calculated incident rate for metacarpal fractures [2]. The fifth metacarpal fracture alone contributes the most to this category. Unlike hand or wrist fractures that occur due to a fall onto an outstretched hand, an injury to the fifth metacarpal occurs mostly due to a direct impact or trauma exerted on the metacarpal bone in a clenched position. The most common place for such injuries is within the home environment, followed by athletic and recreation-related activities [1][2][3]. Non- operative treatment is advisable in case of stable fractures, whereas unstable fractures require surgical reduction with fixation supplement [12][20]. For this long bone, treatment with intramedullary devices in several scenarios has gained the attention of clinical research and is sometimes used by orthopedic surgeons. The market place provides a variety of screw designs and sizes for fixation of various bones of upper extremity fracture including carpal, metacarpal, wrist and, phalanx [18]. However, the efficiency of these intramedullary devices is still lacking consensus when it comes to fixation of the fifth metacarpal bone [20]. Existing techniques have been criticized for violating articular cartilage or obstructing the metacarpophalangeal joint. Different pitches of the screws have been highlighted for

compressing and reducing the length of the metacarpal. Some devices offer rotational stability but can result in intra-articular surface migration [20][21]. The intramedullary (IM) devices are suggested to be used as compressive struts inside the intramedullary canal. IM devices within the central line of the canal can position better than plates for fixation. They can resist bending from more than one direction and hence stabilize the long bone fracture. It is important for the IM device to have optimal contact with the internal cortex to resist torsional and shear stress. This can be achieved when the nail positively engages with the intramedullary canal without disrupting blood supply since tightfitting nails could negatively impact the regeneration of medullary circulation [31]. Some literature also highlights the limitation of placing an intramedullary device without reaming and only in contact with the narrowest portion, the isthmus [18]. Studies indicate that there are conflicting guidelines from physicians and limited literature to suggest the best treatment algorithm [3]. Hence, there is a requirement for morphometric analysis which may aid in designing intramedullary devices. Also, there is no study conducted so far to highlight the density distribution in the metacarpal bones. Hence, this study can build a foundation for the analysis of the density distribution of the metacarpal bone, and establish a relation between the bone density distribution and thickness, for future research.

1.2 Study Aims and Objectives

This study focused on the morphometry of the fifth metacarpal bone, due to the limited literature in this area and the surgical treatment modalities available today. The derived parameters from the morphometric analysis could be used to optimize the dimensions of intramedullary devices in the future [3]. In addition to this, the study sought to explore if there

are any gender-related variability or other correlating factors in morphometry. Data collection for this study was performed by 3-dimensional scanning of cadaveric hands. Only a previous study by Michael Rivlin et al. [14] has utilized 3D CT scans to study dimensions of metacarpals. The study reconstructed images in three planes to achieve an orthogonal view [14]. The 3-dimensional computed tomography helps in true 3D geometry analysis without positioning-bias of the subject, and the noninvasive osteo-absorptiometry method helps to analyze density distribution of the bone.

This study aimed to calculate the inscribed and circumscribed circles for both solid and canal model of the fifth metacarpal which could help verify the optimum fit for the IM devices for that bone. For universal measurement and scaling; and defining data points for the scribed circles for bone model, principal component analysis (PCA) was applied. The PCA method of analysis was adopted from the study by Jasmine Aira et al. [25] where the morphometric analysis of the clavicle intramedullary canal was conducted. Further, as a part of the density study, the methodology used by Peter Simon et al. [24] for reviewing subchondral bone density distribution in male total-shoulder arthroplasty subjects was customized to fit the analysis of density distribution of the fifth metacarpal bone. In that shoulder study, the glenoid surfaces were manually traced in the axial view. The Hounsfield (HU) values for the surfaces were considered for density distribution and its analysis. The details of the procedure followed are mentioned in the methodology section of chapter 3.

1.3 General Limitations

The specimens collected were predominantly older adults, with an average age of 70 years. The information on hand dominance for cadaveric specimens was unavailable. Hence, demographically the data was focused on gender only. The two anatomical sides of the hands were not from the same specimen. Hence, drawing a conclusion based on the comparison of the right and left side of the hand from different specimens would be inaccurate.

Chapter 2: Background

2.1 Fifth Metacarpal

The metacarpal bone is divided into three regions: head, shaft (neck and body) and, base (see figure 1). The bone characteristically has concavity on the palmar surface [3]. The fifth metacarpal attached to the small finger (fifth digit) is the second shortest bone among the metacarpals. The base has a strip articular facet along the lateral surface and a non- articular tubercle toward the medial side. It also has a slope towards the proximal ulnar side. These patterns on the base region can also help in identifying the anatomical sides of the fifth metacarpal bone (whether the bone is a part of right- articulated or left- articulated hand). The quadrilateral articular surface in the bottom of the base articulates with the distal articulate surface of the hamate carpal bone [4][5]. This joint is saddle-shaped due to the grooves at the hamate surface which facilitates it to hook at the distal position of the carpal. At the distal end of the fifth metacarpal i.e., head, the articulation surface is larger than that of the fourth metacarpal. The articular head is more prominent towards the volar side [4].

The metacarpal bones of four digits together form a transverse arch which gives shape to the palm and required support to hand for conducting the gripping or lifting task. Some of the metacarpals have a spur growth around the lateral or medial condyle of the metacarpophalangeal joint called sesamoid. A sesamoid is a normal variant and does not represent osteoporosis or osteoarthritis. The articular surface in the base of the fifth metacarpal

connects with the fourth metacarpal bone. The mobility of these two bones together forms a movement also known as encompassment [4].

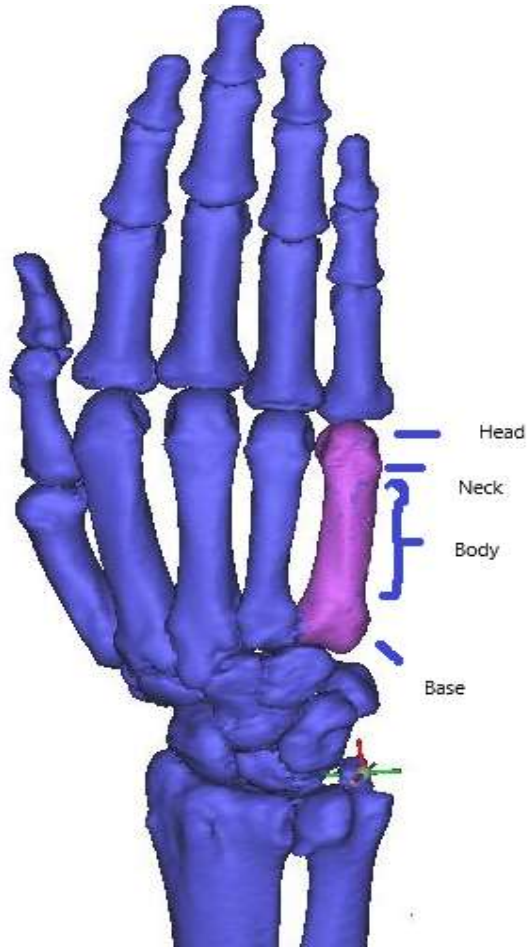

Figure 1: 3D model of hand (right anatomical side) from MIMICS (Materialise, Leuven, Belgium).

2.2 Ligaments and Other Associated Structures

The non -articular tubercle surface on the medial side of the base provides attachment to the pisometacarpal ligament and insertion of tendons of the flexor and extensor carpi ulnaris muscle [3]. The vertical ridge of the shaft in this long bone divides it into two regions. The lateral part between the fourth and fifth metacarpal serves as the attachment for the dorsi interosseus muscles. The medial dorsal side of the bone has a smooth and triangular-shaped surface, which provides attachment to the extensor tendons for the small finger. The anterolateral surface of

the shaft serves as the origin of the palmar interosseus muscles. The metacarpophalangeal (MCP) joint flexion is primarily controlled by the interosseous muscles along with lumbrical muscles. The metacarpal head shape helps to form the condyloid joint with the proximal phalanx [4]. During the hand extension and flexion, collateral ligaments of the MCP joint provide stability for a lateral key- pinch and grip strength. The volar plate and flexor tendon drive extension as well as resist hyperextension at MCP joint. Additionally, the intermetacarpal ligament helps to stabilize the fingers, minimizes proximal migration and rotation in the case of a fractured bone. The ring and small fingers are comparatively more flexible than other metacarpals due to flexion-extension arc motion, which varies up to 15^{o}-25^{o} at the carpometacarpal (CMC) joint between the fourth and fifth metacarpal and hamate [3]. The first metacarpal that articulates with the thumb is an exception to the rest of the metacarpals.

2.3 Fractures of Fifth Metacarpal Bones

Metacarpal fractures constitute 18–44% of all hand fractures, with the fifth finger being most commonly involved [1][3][8]. The study by Sherif Galala and Wael Safwat [10] states that fifth metacarpal bone fractures account for 38% of the hand fractures. During activities like punching, energy is transferred from a clenched fist to the metacarpal bone axially. Such exertion leads to apex dorsal angulation due to the forces exerted by the pull of interosseus muscles [1]. The fracture impact is measured as the degree of displacement, rotation and angulation along with the fracture type: i.e. transverse, oblique, spiral, comminuted, impact or avulsion. The acceptable apex – dorsal angulation of fracture for the index and middle finger is 15^{o}-20^{o},

whereas, for the ring finger and small finger it is 30^{o} and, 40^{o} respectively. However, during a shaft fracture, CMC joint recovery threshold is 15^{o} without functional impairment [3].

The neck fracture of the fifth metacarpal by itself, also known as a Boxer's fracture, forms about 10% of all hand fractures. Boxer's Fracture is a common type of injury among men within the age group of 10-30 years [1]. Some literature also highlights comparatively rare stress fracture in the fifth metacarpal among athletes. Such fracture might happen when external forces combine with internal forces of muscles. Its diagnosis is considered when there is persistent hand pain while performing any sorts for gripping activity [6][13]. Similarly, "mirrored" Bennett's and Rolando's fractures, both of which are intra-articular fractures, occur when there is an intense pull of the muscle extensor carpi ulnaris leading to subluxation of the dorsal fragment at the base of the fifth metacarpal [7].

Apart from a fracture, CMC- joint dislocation can result in carpometacarpal joint arthritis. Being a scenario as rare as 1% of all hand fractures, CMC joint injury diagnosis often gets missed during physical examination [28].

2.4 Current Methods of Diagnosis

For fracture evaluation, edema, and possible deformities like lost knuckle contours or prominent bony shape at proximal dorsal side due to angulation, and the location of complained pain should be considered. In addition to comparing contralateral hand, excessive angulation should be assessed radiographically in different views (posterior-anterior, lateral and oblique) to advise on the method of treatment. Along with all fracture examination, a neurovascular examination is pertinent to check for sensation, motor function, and blood flow [1]. Computed

tomography method is unlikely to be used unless there is a high degree of clinical suspicion on a negative plain radiograph. However, some literature suggests that accuracy in measurements of deformity can help determine the appropriate course of treatment [1][14].

2.5 Current Methods for Treatment of Metacarpal Fractures

2.5.1 Nonsurgical Treatment

In case of Boxer's fracture with bruised knuckle and concomitant injuries, the wound should be disinfected thoroughly. If it is a closed or displaced fracture with no excessive angulation, splinting can help for immobilization of joints. In many cases of the fifth metacarpal fracture up to 30^{o} of angulation, the conservative treatment without reduction suffice for the healing process [1]. However, the study by Yueng Cheng et al. [8] states, with non–operative treatment for dorsal angulation, the chances of volar malunion and stiffness are high.

2.5.2 Surgical Treatment

Complexities like intra-articular fractures, unstable open fractures, segmental bone fractures are indicative of operative treatment. It is necessary to correct any malalignment, for which the surgeons generally rely on the stable MCP joint to aid corrective action on rotational alignment. The conventional treatment methods for fractures are implant of plates and screws, dynamic compression plate, and intramedullary devices. There is some literature available comparing the transverse pinning and intramedullary pinning [3][8][10]. Transverse pinning takes shorter operative time and has less incidence of complications. There is also literature available on a variant of transverse pinning of metacarpal bone - open reduction and internal fixation

(ORIF). ORIF is being used for treating multiple fractures that require high mechanical stability. In this method, a K-wire is integrated with cerclage wire, which is cost-effective and causes lesser tissue damage than plate fixation [8]. However, the strength of K-wire used in traverse pinning fixation is limited. On the other hand, the plates and screw fixation restrict the motion and are associated with avascular necrosis [3]. In other techniques, Dr. Foucher introduced the method "bouquet", which is closed antegrade nailing of metacarpal fractures using multiple small pre-bent K- wires. The benefit of this technique being, it does not require opening the fracture. However, it is a difficult procedure to perform due to proximal surgical incision [9]. Many authors have suggested that IM pinning improves motion and requires less shortening for bone. Intramedullary fixation of metacarpal shaft fractures using small flexible rods and headless compression screws have been recognized to provide stable internal fixation while minimizing the extent of soft tissue injury [9][20]. The paper by Jorge Orbay also suggests IM nailing with the combination of proximal locking could expand the scope of treatment to spiral and comminuted type of fractures [9]. Antegrade intramedullary device fixation has also been used successfully and offers limited soft tissue damage but the nail can potentially migrate into the metacarpophalangeal joint [12]. The procedure requires removal of the implant after fracture healing. Some literature discusses the potential risk of infection or broken hardware due to the headless screw [3][11]. Again, a headless screw-end can obstruct and restrict the MP joint rotation. The study by Doarn, Michael C et al. highlights and favors the newer technique of retrograde headless intramedullary fixation [12]. In this technique, screws were placed dorsally in the metacarpal head to align with the intramedullary canal. The longest screw sizes had a preference with variation in screw thread- long in neck fracture and short threads in shaft

fractures. In this procedure, the screw was buried within the subchondral bone [12][21]. The head fracture often involves articular surfaces, where if the fracture is comminuted, the repair is not plausible. Hence replacement arthroplasty or arthrodesis is suggested [3].

2.6 Previous Morphometry Studies

The morphometric analysis of the fifth metacarpal helps in pre-operative templating and determining the dimension of the canal which would guide the choice of screw size. [20] Attributes to be considered for analysis are the bone radius of curvature, medullary canal diameter, cortical thickness and narrowest portion of intramedullary canal, that is isthmus. There is literature available on morphometry studies with parameters like the shaft length, shaft bending angle (SBA), and capital axis angle (CAA).

Michael Rivlin et al. [14] used 3 D images in sagittal and coronal projection to present the posteroanterior and lateral view in 2 Dimensions, which later was utilized in leu for orthogonal view. The length of the shaft was calculated as the distance from the center to two extreme ends of distal condyles. However, the various angle calculation was subsequently summarized to conclude minimal bending angle of capital axis angle is averaged to 12^{o} and the shaft bending angle from apex to dorsal is 10^{o}. From posterior-anterior images, the fifth metacarpal was observed to be almost straight. Berg et al. [15] utilized 16 CT scans to create a 3D model of the metacarpal bone and inserted a 3D replica of a screw and utilized volumetric analysis to measure volume occupied by the portions of interest of the screw. It illustrated virtually simulated retrograde IM insertion through quantitative 3D CT. To assess the articular starting point of insertion, surface area and subchondral volumes of the head were used during headless

compression screw fixation of the metacarpal bone. For this study, the data of neck fractures were exported to MATLAB for simulation. This study quantified the extent of violation by the retrograde headless screw. It highlighted a surface of 129 mm^2 area mated between the proximal phalanx and metacarpal head through the coronal arc and 265 mm^2 area through the sagittal plane. Hence concluding that while using a 3 mm headless compression screw, a total of 8% and 4% of the surface mated in the coronal and sagittal plane, respectively. George Lazar et al. [16] studied the structure of the intramedullary canal of metacarpals with the help of the 2D radiographic method, and Vernier caliper. The data were collected to define the shape of the metacarpal cadaveric bones. Their research emphasized the importance of the shape of the intramedullary canal from the transverse section which affects the choice of IM device. Results concluded that the medullary canal of second, third and fourth metacarpals are more oval than the fifth metacarpal which is nearly round. It also states that due to the variation in thickness of the cortical wall in different directions, the IM device should be fitted dorsally. The result of subjective observation in this study stated the diameter of the intramedullary canal to be 4.3 mm (±1.0). and 4.2 mm (±1.1). from frontal and sagittal views respectively.

J, J Vaux et al. [22] conducted the human thumb metacarpal morphometric analysis with a total of 80 metacarpals from 46 cadavers. For each bone, a virtual 3D model was constructed by reviewing the sagittal, coronal and lateral plane of CT scans. The bones were analyzed for the overall length, the radius of curvature and distance from the narrowest portion of the intramedullary canal. This morphometric study was done with the intention to use that data for osteointegration in cases of thumb amputation. The limitation of this study was in the accuracy

of locating the narrowest portion of the thumb, manually. The manual process in CAD application could have some level of observer bias.

In terms of the density analysis of the fifth metacarpal, there is very limited literature available. There is literature that suggests the relative association of the fracture risk to volumetric bone mineral density [30]. There is also a study available by Irene Llorente et al. [17] which devised bone mineral density analysis of the cortical bone for predicting the extent of arthritis. This study used conventional dual X-ray absorptiometry for studying the third metacarpal radius, and tibia of rheumatoid arthritis patients. The results highlighted 75.7 mm^2 of total cross-sectional area, and 1,166 mg/cm^3 of volumetric bone mineral density in the shaft location of third metacarpal bone, which constitutes 30% of the total volume of bone.

There is no study conducted so far to highlight the density distribution in the metacarpal bones. However, the literature suggests that Hounsfield's unit scale is a useful "surrogate marker for bone mineral density" [29]. In other studies, spatial mapping of humeral head bone density by Hamidreza Alidousti et al. [23] used CT scans of 8 cadaveric humeri for predicting the bone density distribution. The scanned images were processed in MIMICS to generate the HU format file of the humerus head. These files were imported in MATLAB for density analysis. In MATLAB, centroid was calculated for each specimen and assigned the corresponding bone density. The data was sorted to divide the humeral head into 12 slices parallel to the neck of the respective humerus bone. Each slice was then divided into 4 concentric zones. The bone density used an average of subvolumes of the point cloud. Though the method ensured these values did not overshadow the variation in local properties, it could still not distinguish the bone in the 4^{th} concentric zone.

In the density distribution analysis of glenoid surfaces by Peter Simon et al., [24] the HU values for the surfaces were accounted up to a depth of 5 mm. The surfaces traced were as per the position of the pixel considered for the edges. Thereafter the glenoid zoning was performed by defining the central zone as concentric part. The study highlighted that the zonal analysis of density distribution could be an effective tool for preoperative planning. High density in the concentric part and posterior zone in the peripheral area suggested the pattern of cartilage loss in the peripheral area during the progression of osteoarthritis.

Chapter 3: Methodology for Morphometry and Density Analysis of the Fifth Metacarpal

3.1 Study Population

An a-priori power analysis determined a minimum sample size of 12 specimens per gender group is required to show gender differences in overall length (90%, large effect=0.8). For this study, hands were harvested from cadavers and scanned via computed tomography. Post - scanning, the CT scan images were clinically screened by orthopaedist Dr. Shaan Patel from Morsani College of Medicine (USF) for osteoarthritis at carpometacarpal and metacarpophalangeal joints. The aim of this morphometric analysis is to list the dimensions of an average healthy fifth metacarpal bone. There were 22 males and 16 female samples. The average age of the collected specimens was 70 ± 13 years (71 ± 12.8 years for male; and 69 ± 13.7 years for female). Average height was 170 ± 12 cm (177 ± 12 cm for male and 159 ± 12 cm for female); average weight was 68 ± 18 kg (76 ± 18 kg for male and 57 ± 18 kg for female), and average BMI was 23 ± 5.4 (24 ± 6 for male and 22 ± 5 for female). There were in total, 4 left and 12 right hands for the female population and 10 left and 12 right hands for the male population considered as per the study's selection criteria.

3.2 Methodology

The acquired 3 D CT scans were in axial view, with the length of the long bone to be the Z-axis. The cadaver hands were spaced in the GE lightspeed scanner in such a way that images

could be captured with the required scale, 0.625 mm of thickness and pixel size of 0.383- 0.619 mm. The images were then stored on the DICOM system (Digital imaging and communications in Medicine) to be transferred to the MIMICS application platform.

3.2.1 Segmentation

For each specimen's hand, the image was individually processed as illustrated in figure 2.

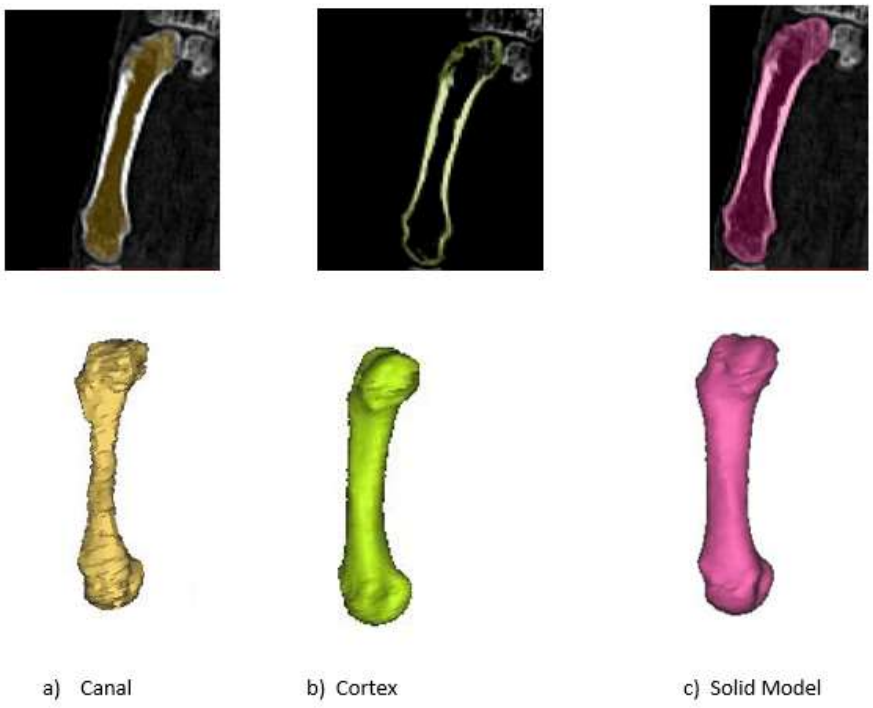

Figure 2: Image processed for the fifth metacarpal bone from CT scan. a) Volumetric model of the canal, b) Cortex model and c) Volumetric model of whole fifth metacarpal.

The threshold value in the Hounsfield scale was set as per the cortical bone region on MIMICS to define the initial contours. Each image was modeled for its whole solid shape and canal section separately. The cortical portion was then generated by subtraction of the canal from the solid model, using the Boolean operation. This function was performed to avoid

redundancy as well as miss out on any of the modeled regions. All three generated models were then exported in both point cloud (PC)and Hounsfield (HU) format**.**

3.2.2 Coordinate System and Alignment

The hands were scanned in the prone position hence establishing the Z-axis along the length of the bone. Axis X & Y were identified via transverse and coronal views of the model. The axes identified by these views were not aligned with the global coordinate system. The principal component analysis was used to align the axes of these models for geometric interpretation. PCA utilizes a matrix of data points to find the eigenvector and eigenvalues. The principal component is said to be a linear combination of the original data points. In the newly formed coordinate system (global coordinate system), the first principal component axis is in the direction of the greatest variance of data points. Consequently, the second and third eigenvector would be orthogonal to the first principal component. Hence, yielding longitudinal axis 'Z' (1^{st} principal axis), anterior-posterior direction 'Y' (2^{nd} principal axis) and lateral – medial direction 'X' (3^{rd} principal component).

For PCA and further morphometric and density analysis, the point cloud and Hounsfield format files generated on MIMICS are imported onto MATLAB (MathWorks, Natick MA). The algorithm from the previous study by Jazmine Aira et al. and Peter Simon et al. was opted and customized to fit the requirement of our analysis [24] [25]. The normalization and alignment are pre-requisite to further analysis for both morphometry and density distribution.

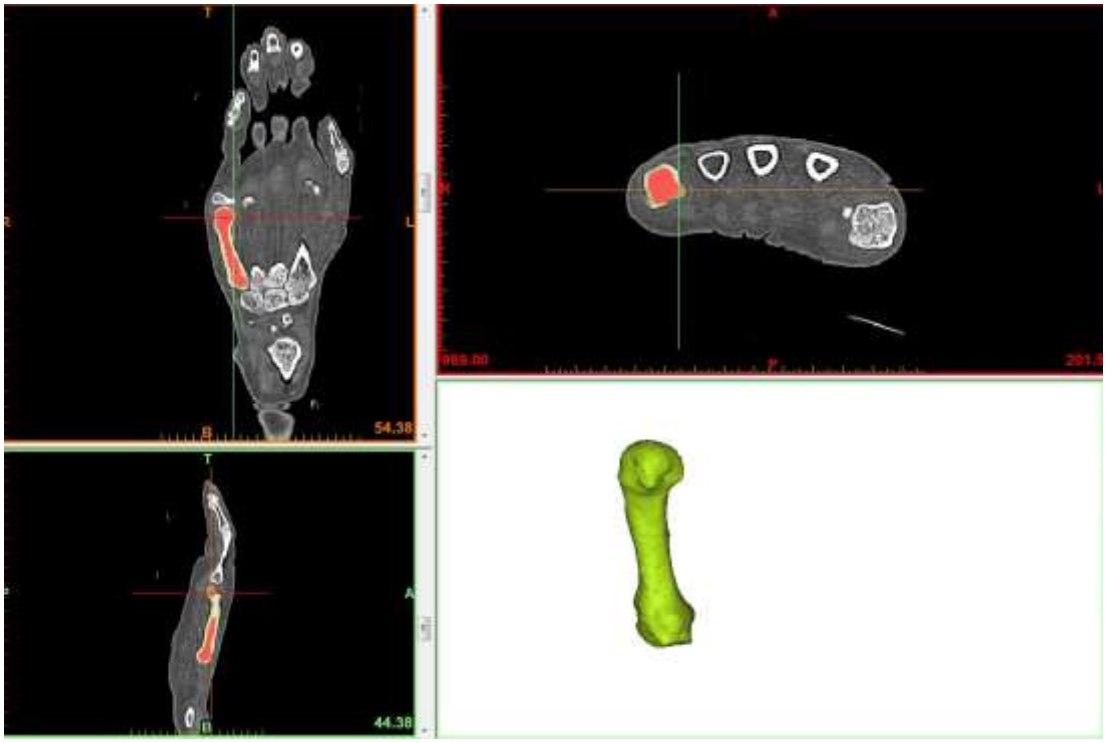

Figure 3: The image from MIMICS. Starting from top right corner clockwise is the Transverse section, complete model Fifth Metacarpal, sagittal view and coronal view. The longitudinal axis along the length is established as Z-axis.

3.2.3 Normalization

Before morphometric analysis, every fifth metacarpal model underwent normalization to transform from the local coordinate system to the global coordinate system. The technique used for the normalization of coordinates is principal component analysis. Firstly, the geometric center was calculated by finding the volumetric mean of the solid shape of the fifth metacarpal, and canal model, individually.

$$C_x = \frac{1}{N}\sum_i^N xi; \quad C_y = \frac{1}{N}\sum_i^N yi; \quad C_z = \frac{1}{N}\sum_i^N zi$$

In the next step, every model was translated from their geometric center [Cx, Cy, Cz] to global origin [Gx, Gy, Gz] and aligned with the three principal component axes. To align models with the created principal component axes, we applied orthogonal rotation from the local

coordinate system to the global coordinate system. Hence completing the orthogonal transformation.

1) Translation:

$$\begin{bmatrix} Gx \\ Gy \\ Gz \end{bmatrix} = \begin{bmatrix} Lx \\ Ly \\ Lz \end{bmatrix} - \begin{bmatrix} Cx \\ Cy \\ Cz \end{bmatrix}$$

2) Rotation:

$$^{G}_{L}R = \begin{bmatrix} P3 \\ P2 \\ P1 \end{bmatrix} \begin{bmatrix} Gx \\ Gy \\ Gz \end{bmatrix} = \begin{bmatrix} P3.Gx & P3.Gy & P3.Gz \\ P2.Gx & P2.Gy & P2.Gz \\ P1.Gx & P1.Gy & P1.Gz \end{bmatrix}$$

As a control to maintain the consistency in data, all the included left hands were verified and vertically inverted (not mirrored) along the Z-axis.

3.2.4 Measurements

To verify a holistic measurement of length, the bounding box function was applied to Hounsfield format of the solid model (see figure 4). The bounding box function calculates the maximum and minimum values of the tightest-fit for the bone model. The next section explains the algorithm considered for measurements for the scribed circle of the canal and the whole fifth metacarpal model (the solid model) as well as the density distribution of the bone.

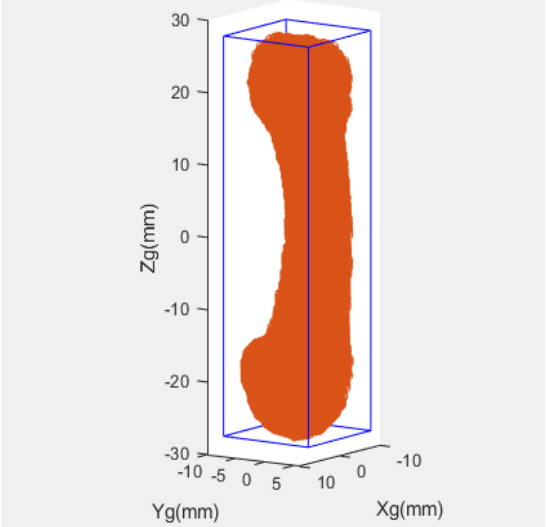

Figure 4: The solid model of the fifth metacarpal after orthogonal transformation.

3.2.5 Inscribed and Circumscribed Circles Calculation

The models were then sectionalized in 50 planes along the length (Z-axis), which later were utilized to draw 3D circles (inscribed and circumscribed) for both solid and canal model, individually. The circumscribed circles were drawn with minimum radius, which could enclose the complete set of points (X, Y) along the Z-axis, on the surface of the canal and solid model, individually at a particular section. To ensure that the maximum number of point projections were being utilized for every section, the points between the consecutive planes n and n+1 were merged and flattened on a single surface. This function was performed at all 50 planes of the model. The ellipse geometry is conditioned to at least pass through 3 points set to draw the circumscribed circle.

For the two sets of models, the inscribed circle was also drawn for the polygon [x,y], using the Voronoi diagram. Again, the Voronoi diagram is drawn with at least 3 input points, which partitions the plane into specific regions as per distance of a seed to its subset points (which are

in proximity to that seed). Hence, the Voronoi edge is defined by two adjacent Voronoi regions, equidistant from two seeds. Subsequently, the intersection of three regions is a Voronoi edge which is equidistant from the three seeds. The Voronoi diagram is created around the Convex Hull of point cloud surface in a cross-section.

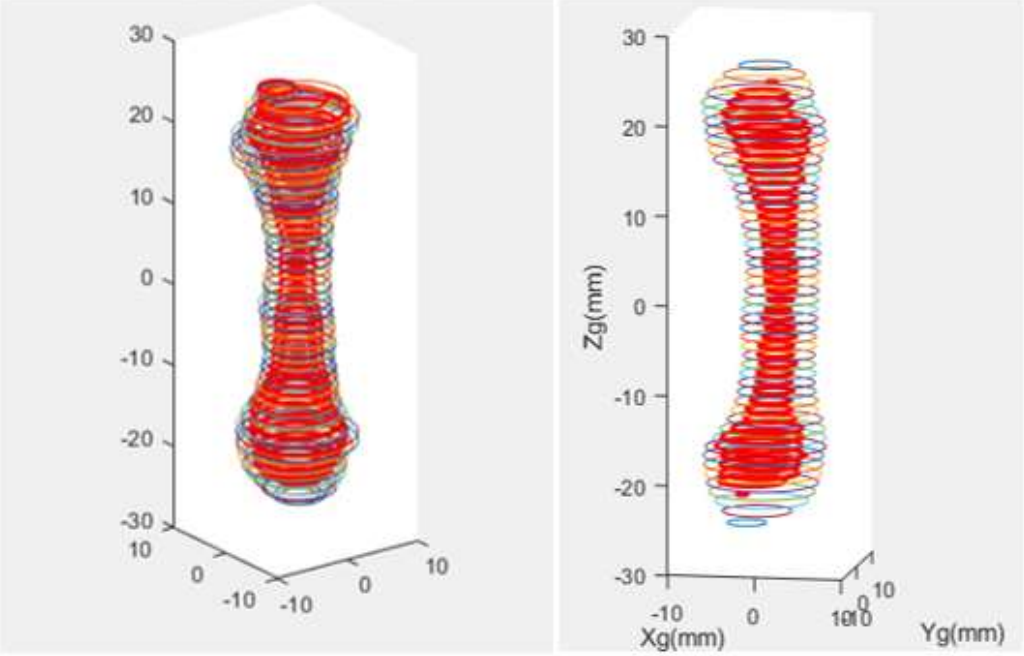

Figure 5a: The bone model with the circumscribed circle around solid HU model, and circumscribed circle around the canal HU model.

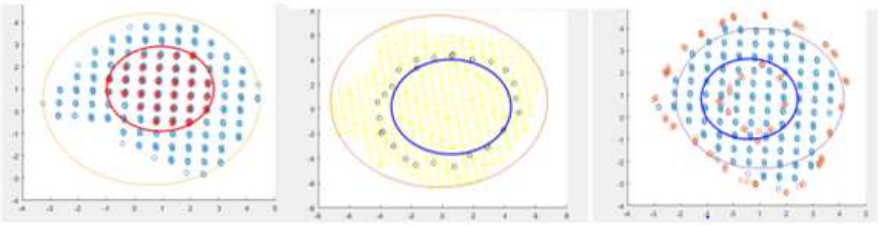

Figure 5b: The cross-section of the 3D scribed circles drawn around the two models in possible combinations.

In this manner, four models generated with the stated algorithm are:

1) Circumscribed circle of solid HU

2) Inscribed circle of solid PC

3) Circumscribed circle of canal HU

4) Inscribed circle of canal PC

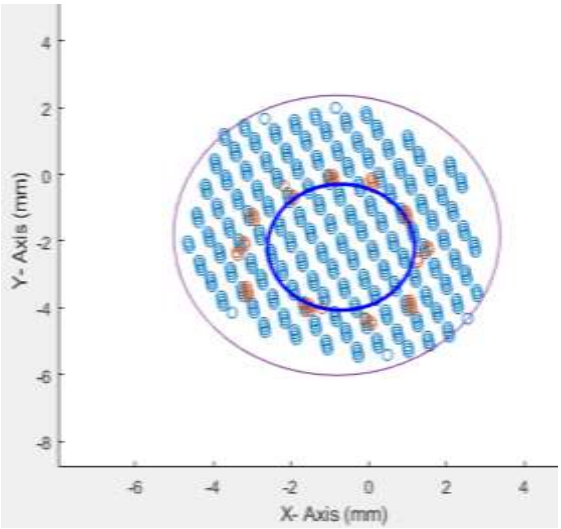

Figure 6a: The cross-section of the solid HU model with the circumscribed circle and canal PC model with the inscribed circle.

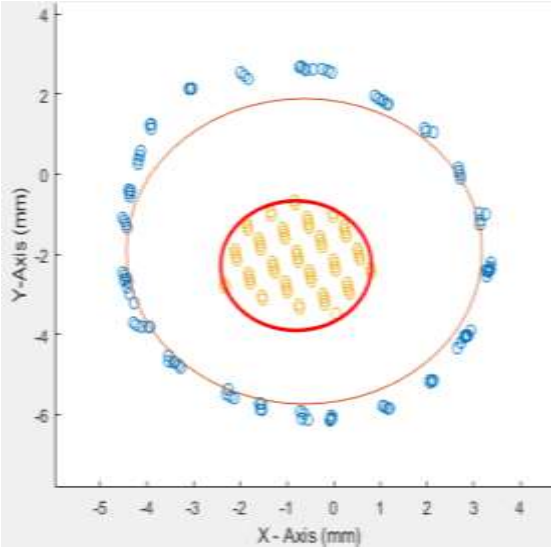

Figure 6b: The cross-section of the solid PC model with the inscribed circle and canal HU model with the circumscribed circle.

This study has explored the efficiency of automated evaluation of dimensions of the fifth metacarpal bone. The detailed flow charts of the morphometric analysis below depict the automated process applied for measurements.

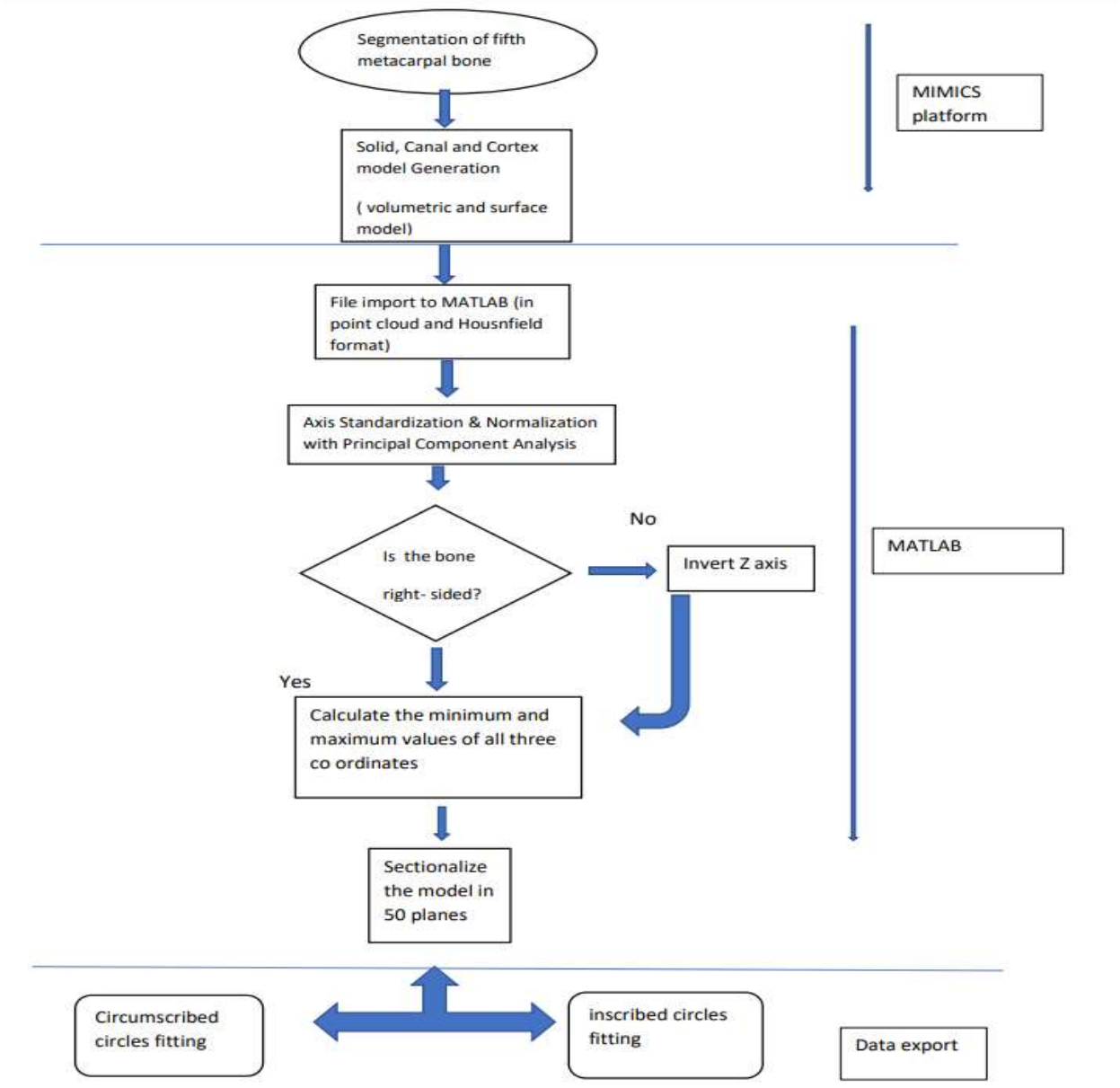

Figure 7: Flow chart diagram.

3.2.5.1 The Efficiency of the Algorithm

The study by Michael Rivlin et al highlighted the capital axis angle and the shaft bending angle for the fifth metacarpal bone [14]. Hence, it became imperative to analyze the deviation of the critical data of inscribed circles for the canal model. For the analysis, the mean squared error of every center of 40 planes was calculated. This helped substantiate the estimation error of the central line as 0.88 mm for X coordinates and 0.86 mm for Y coordinates. The geometry of the fifth metacarpal bone is not perfectly cylindrical. Also, at each plane, a circle or any regular polygon cannot define the dimensions of that cross-section. Furthermore, calculations were performed to determine the average differential distance of points at the surface of the canal model for a cross-section, with respect to the inscribed circle of the canal model at that cross-section. The Average of Absolute value of differential distance was calculated as:

$$(\sqrt{(X-X')^2+(Y-Y')^2})^2-R$$

wherein (X', Y') are the coordinates for the center of the inscribed circle. And, (X, Y) represents the points on that plane. The values were calculated for the 5^{th} to 45^{th} planes of the canal. The irregularity of shape for the internal canal is extremely high for the subchondral region and does not provide significant data for analysis. Hence the values were excluded from the extreme ends of the canal. This analysis for the average of the absolute value of differential distance was run for 3 sample sizes as large, medium and small as per the length of the bone. The differential distance was found to be 1.10 mm, 0.92 mm and, 0.75 mm respectively. Hence, concluding that the values are comparatively small for the average diameter of 5.92 mm, 4.96 mm, 4.66 mm for their corresponding sample model. These measurements can be utilized for the optimization of dimensions for the fifth metacarpal intramedullary devices.

3.2.6 Density Analysis

The morphometric analysis with only inscribed and circumscribed circles does not provide requisite information to quantify the bone thickness and morphology. Hence, the research progressed with the calculation of the bone density distribution, which could unfold the information of variability in the gender, anatomical side and length of the bone with respect to the bone density distribution. The relative density calculation was performed on the cortex model in Hounsfield format. The normalized data was again sectionalized in 50 planes along the length (z-axis), and the elements of the data were converted from Cartesian to polar coordinates. Every section was yet again divided within the 360^{o} angle of the plane, to categorize 2 positive and 2 negative quadrants. The points were then noted from the maximum radius to 60% of the distance towards the center. The interior part of the concentric is defined as the central zone. The intention of zoning is to study the density distribution of the cortex wall for reaming and drilling the intramedullary device inside the bone canal. Hence, the central zone was excluded as being a part of the canal.

The created model was divided into four different zones as per the angular parameter– posterior (135^{o} to 45^{o}), anterior (-45^{o} to -135^{o}), lateral (45^{o} to -45^{o}), and medial (135^{o} to 225^{o}). Such zonal radiodensity value helped to analyze the bone density distribution (see figure 8). The bone density values were collected in the Hounsfield (HU) unit scale, which is a linear transformation of attenuated coefficient measurement with respect to the radiodensity of distilled water.

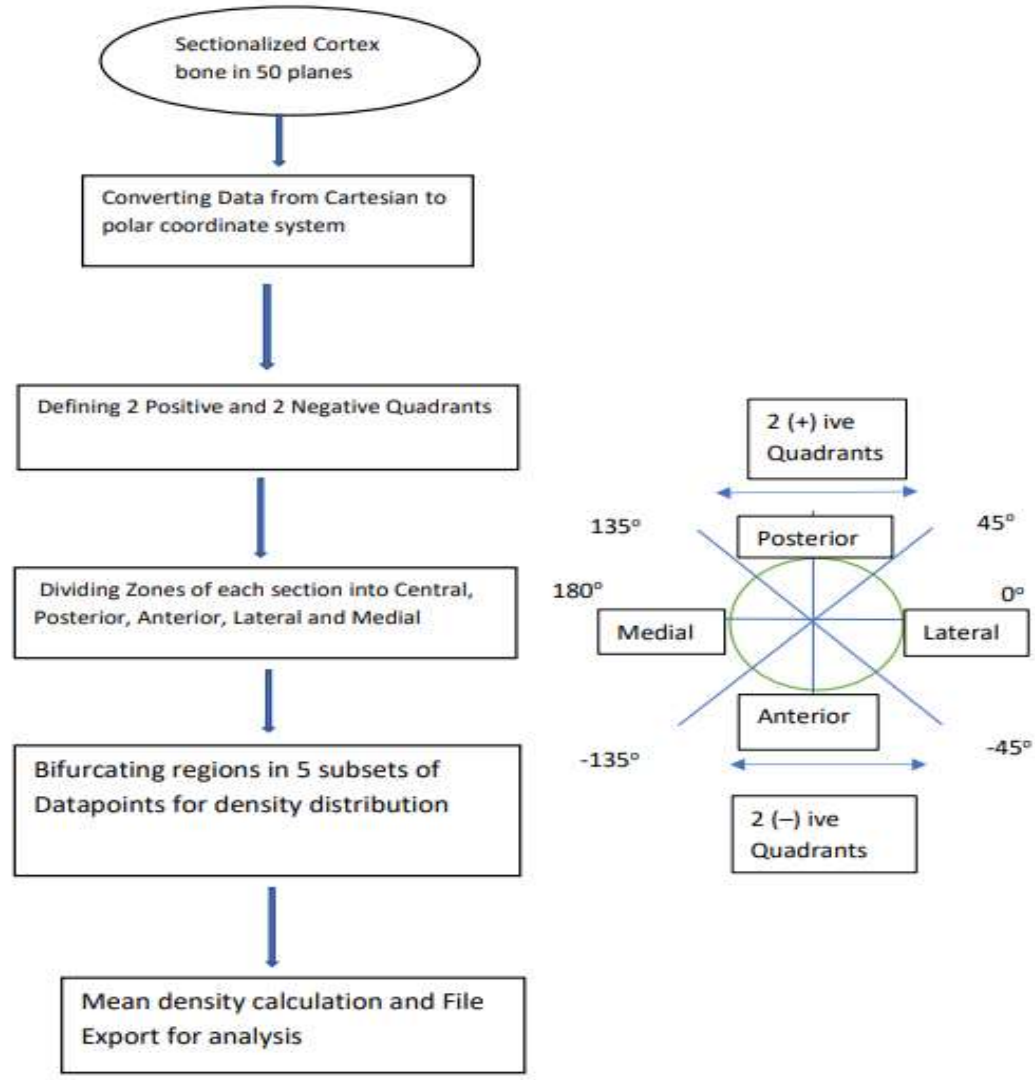

**The Circle in the diagram represents the cross section of the Fifth Metacarpal bone.

Figure 8: Flow chart diagram of density distribution.

The zonal information was further divided in 5 different regions or portions, for a better understanding of bone density distribution at the head, shaft (neck and body) and, base. Such distribution of the high and low density can help in the analysis of the fracture patterns, wherein the location of the fracture can be analyzed to compare the bone density distribution. The data of the mean densities were calculated for all four zones that are posterior, anterior, lateral and medial at each of the divided 5 regions and the total average at that region, separately.

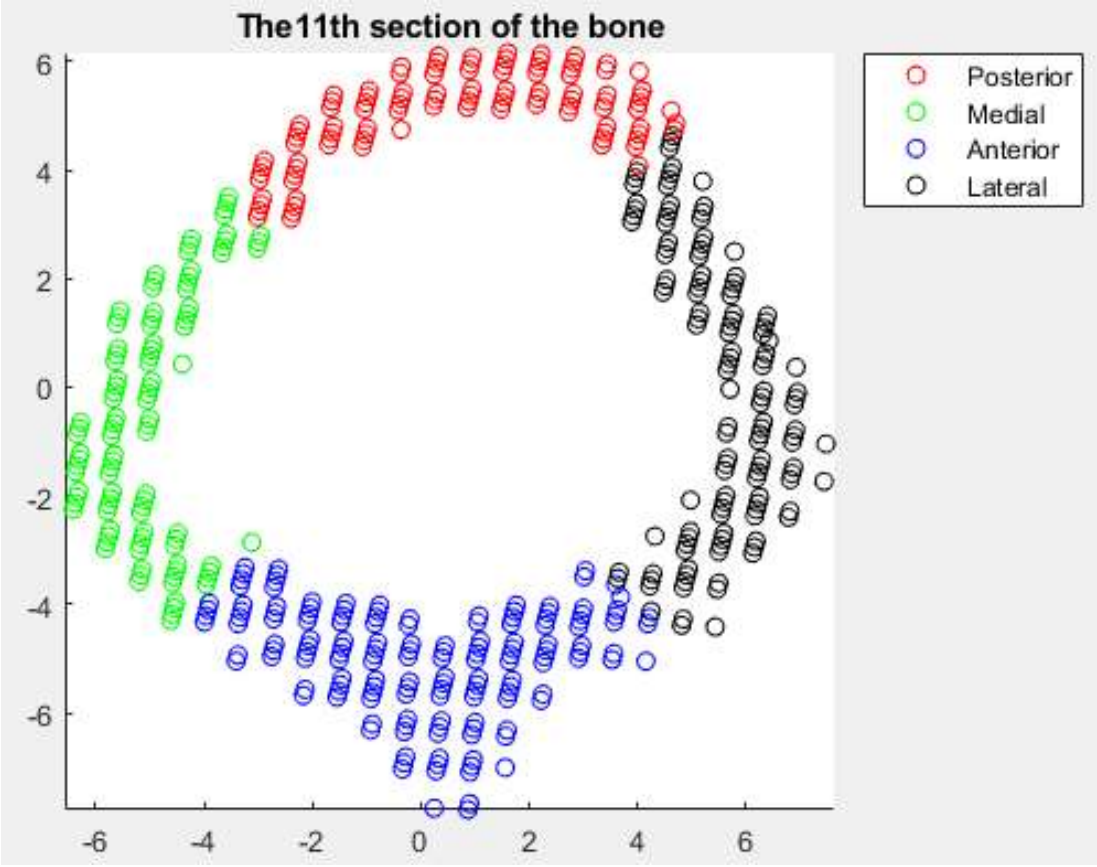

Figure 9a: The cross-section of the neck part of the fifth metacarpal representing the density distribution for the posterior, anterior, lateral and medial side.

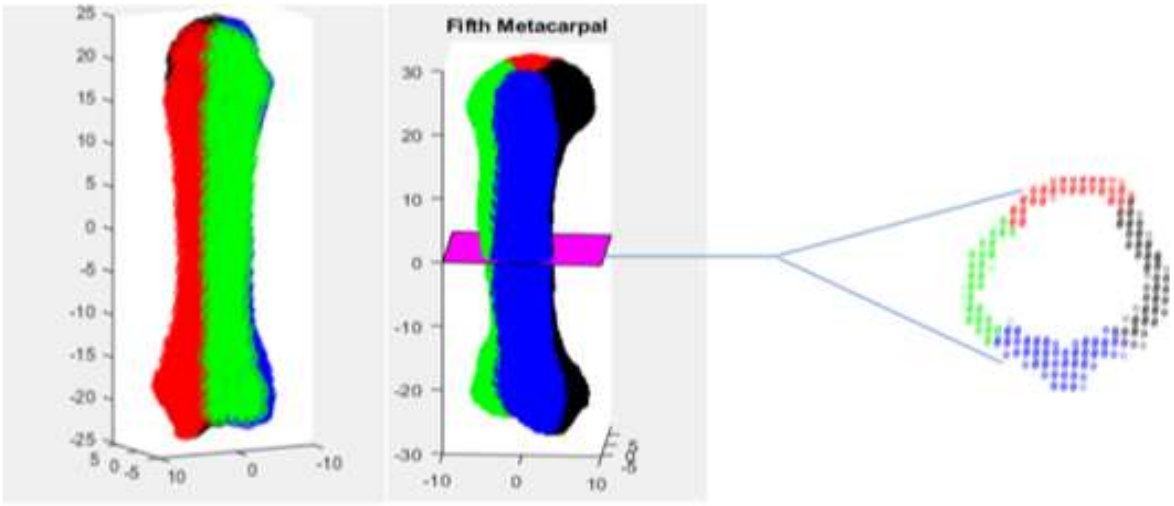

Figure 9b: The bone density distribution of the complete cortical bone.

3.3 Statistical Analysis

For the statistical analysis the average, standard deviation, ranges, minimum values were calculated. In addition to that, a t-test for the gender-wise grouping for four scribed circles and Pearson's coefficient correlation test was performed to find the statistical significance of factor influencing the dimensions of the fifth metacarpal bone. The demographic factors considered for comparison were height, height percentile, weight and, sexual dimorphism. The analysis was performed on SAS software, and the assumed level of confidence was 0.05.

Chapter 4: Results and Discussions

4.1 Results

The diameter of the narrowest portion of the intramedullary canal (isthmus) was calculated by finding the minimum value of the inscribed circle for the canal model and its reference plane was noted. The values considered for the diameter were dataset points from the 5^{th} to 45^{th} planes. Similarly, the minimal value of diameter was calculated for every drawn circles' algorithm. The attributes which were statistically computed with the collected data are as follows:

1) Maximum and minimum values
2) Average of minimum radius
3) Standard Deviation

Starting with the length of the bone, we calculated the length of bone as a function of the height of the donor specimen. The average length of the bone was found to be 54.8 ± 4.4 mm. On gender-wise grouping average bone length for females and males was observed as 50.5 ± 2.1 mm and 57.9 ± 2.5 mm, respectively.

Table 1: Average Length of Bone as a Function of Height of the Specimen Donor.

Height in cm	Average length of the bone in mm with ± SD	
Gender	Female	Male
135-155	50.5 ± 0.9	
155-175	51.3 ± 2.6	55.6 ± 2.9
175-195		59.3 ± 1.3

Overall, the average minimum diameter of the inscribed circle for the canal model was 3.3 ± 0.8 mm at 49.5% of the length. Furthermore, the minimum diameter of the inscribed circle for male is 3.5 ± 0.8 mm, whereas for female it was 3 ± 0.6 mm. Further calculated dimensions have been mentioned below.

Table 2: Average Diameter of Inscribed Circle for Canal.

Average for Female	Std Deviation	Average for Male	SD	Total Average	Std Deviation
3	0.6	3.5	0.8	3.3	0.8
Diameter Mentioned Bone Lengthwise					
Length of Bone	Average Female	Average of Male	Average		
45-48	2.4		2.4		
48-51	3		3		
51-54	3	4	3.4		
54-57	3.4	4	3.8		
57-60		3.2	3.2		
60-63		3.2	3.2		

Table 3: Average Diameter of Circumscribed Circle for Canal.

Average for Female	SD	Average for Male	SD	Total Average	Std Deviation
3.8	0.8	4.3	1	4.1	0.9
Diameter Mentioned Bone Lengthwise					
Length of Bone	Average Female	Average of Male	Average		
45-48	2.8		2.8		
48-51	4		4		
51-54	3.8	4.6	4		
54-57	3.6	5.2	4.8		
57-60		4.2	4.2		
60-63		3.6	3.6		

Table 4: Average Diameter of Inscribed Circle for Whole Bone Model.

Average for Female	SD	Average for Male	SD	Total Average	Std Deviation
5.9	0.8	7	1	6.5	1.1
Diameter Mentioned Bone Lengthwise					
Length of Bone	Average Female	Average of Male	Average		
45-48	5.2		5.2		
48-51	5.8		5.8		
51-54	6.6	6.4	6.4		
54-57	5.4	8	7.6		
57-60		8.4	8.4		
60-63		7.2	7.2		

Table 5: Average Diameter of Circumscribed Circle for Whole Bone Model.

Average for Female	SD	Average for Male	SD	Total Average	Std Deviation
7.8	0.9	9.1	1	8.5	1.2
Diameter Mentioned Bone Lengthwise					
Length of Bone	Average Female	Average of Male	Average		
45-48	6.8		6.8		
48-51	7.6		7.6		
51-54	8.2	9.4	8.6		
54-57	8	10	9.6		
57-60		8.6	8.6		
60-63		9.4	9.4		

As per the t- test analysis (refer tables 6 -9), the gender- wise grouping for the inscribed and circumscribed circle for canal was observed to be statistically significant ($p \leq 0.05$). The circumscribed and inscribed circle for whole bone model was also found to be statistically significant. For the one tail test, the average value of diameter for the male population was hypothesized to be greater than that of average for the female population.

Table 6: Two-Sample t-Test Assuming Unequal Variances for Canal Circumscribed Circles.

	Female	*Male*
Mean	1.88	2.15
Variance	0.15	0.24
Observations	16	22
Hypothesized Mean Difference	0	
df	36	
t Stat	-1.91	
P(T<=t) one-tail	0.03	
t Critical one-tail	1.69	
P(T<=t) two-tail	0.06	
t Critical two-tail	2.03	

Table 7: Two-Sample t-Test Assuming Unequal Variances for Canal Inscribed Circles.

	Female	*Male*
Mean	1.49	1.73
Variance	0.09	0.17
Observations	16	22
Hypothesized Mean Difference	0	
df	36	
t Stat	2.11	
P(T<=t) one-tail	0.02	
t Critical one-tail	1.69	
P(T<=t) two-tail	0.04	
t Critical two-tail	2.03	

Table 8: Two-Sample t-Test Assuming Unequal Variances for Inscribed Circles of Whole Bone.

	Female	*Male*
Mean	2.95	3.48
Variance	0.17	0.25
Observations	16	22
Hypothesized Mean Difference	0	
df	35	
t Stat	-3.56	
P(T<=t) one-tail	0.00	
t Critical one-tail	1.69	
P(T<=t) two-tail	0.00	
t Critical two-tail	2.03	

Table 9: Two-Sample t-Test Assuming Unequal Variances for Circumscribed Circles for Whole Bone.

	Female	*Male*
Mean	3.88	4.56
Variance	0.18	0.25
Observations	16	22
Hypothesized Mean Difference	0	
df	35	

Table 9 (continued)

	Female	*Male*
t Stat	-4.55	
P(T<=t) one-tail	0.00	
t Critical one-tail	1.69	
P(T<=t) two-tail	0.00	
t Critical two-tail	2.03	

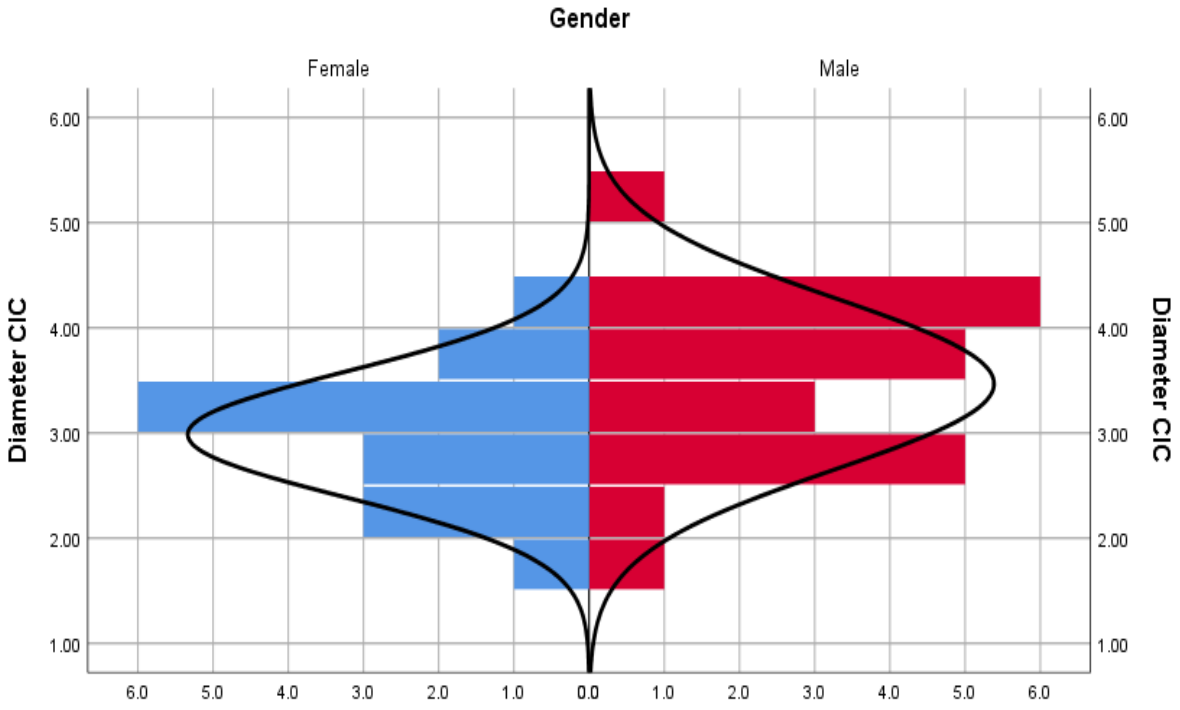

Figure 10a: Population pyramid frequency for diameter of inscribed circle for canal model.

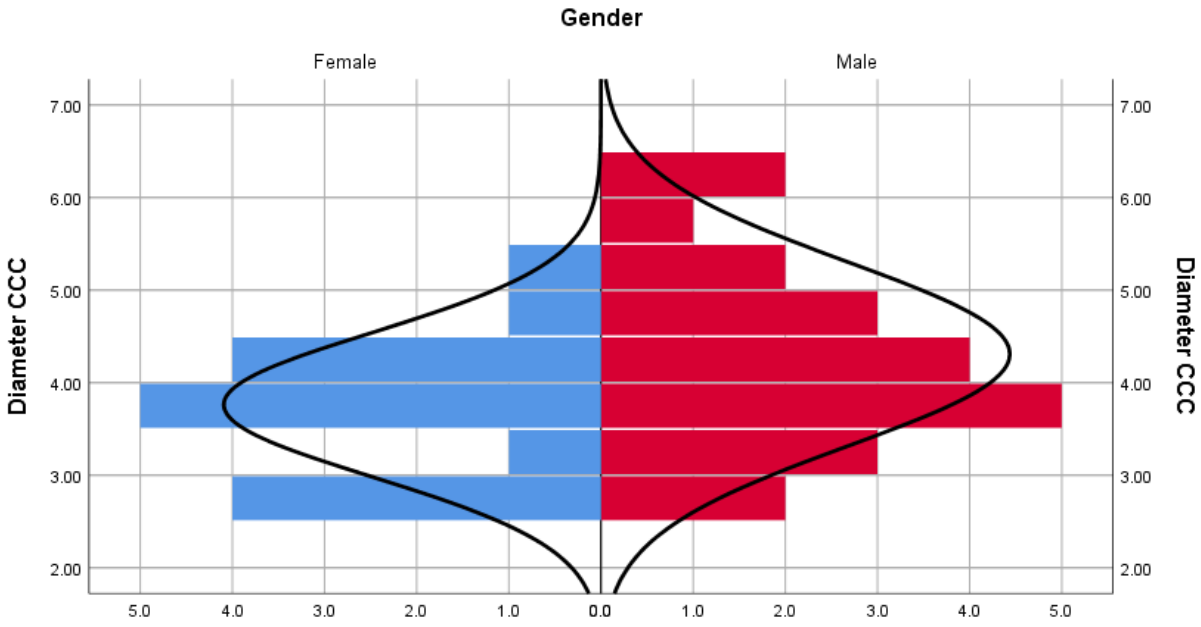

Figure 10b: Population pyramid frequency for diameter of circumscribed circle for canal model.

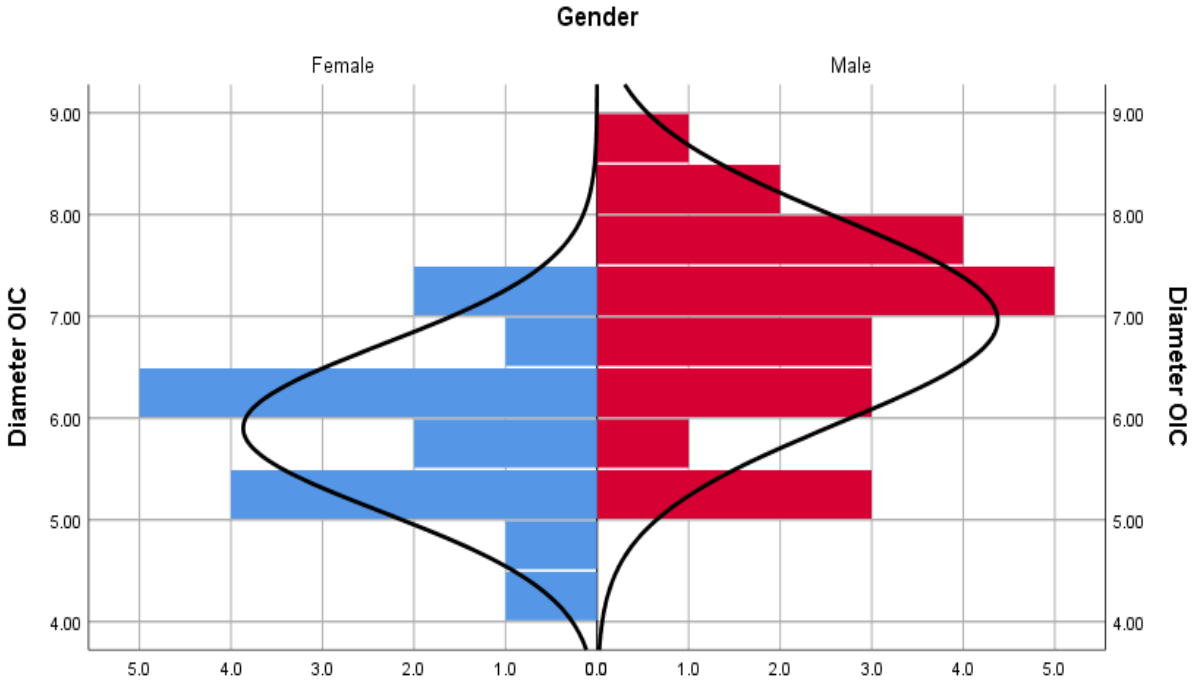

Figure 10c: Population pyramid frequency for diameter of inscribed circle for whole bone model.

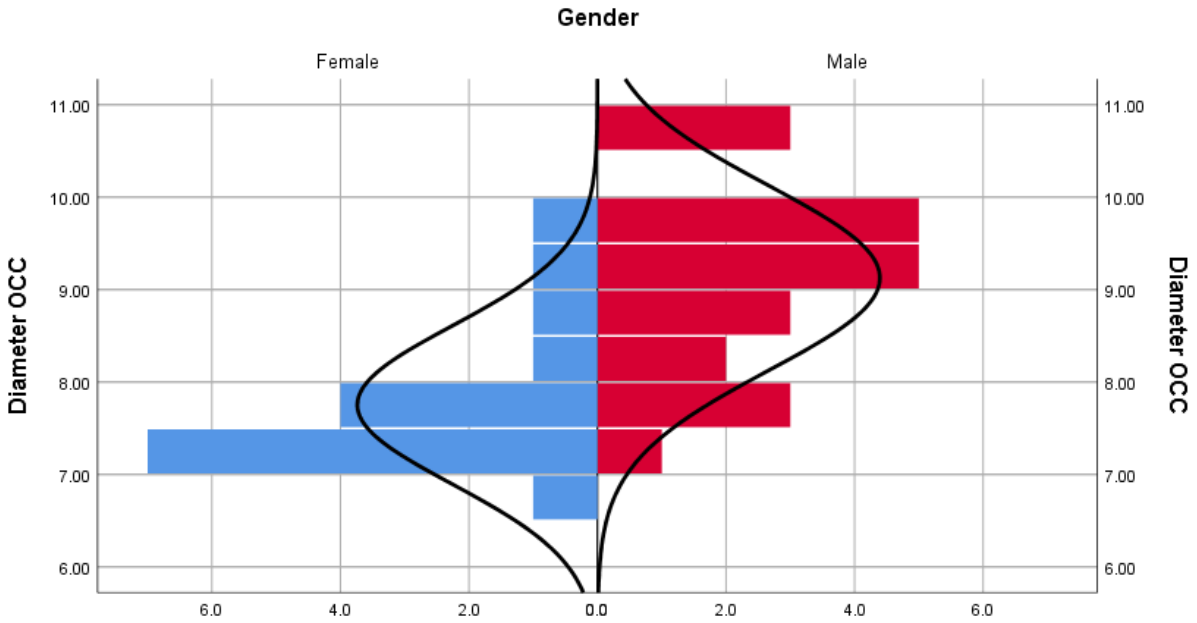

Figure 10d: Population pyramid frequency for diameter of inscribed circle for whole bone model.

The Pearson's coefficient correlation test verified the relation of height with respect to bone length, the diameter of the inscribed and circumscribed circle of the canal. This was statistically significant with a p-value of 0.0294, 0.0743 and 0.0797 respectively in the male specimen. The correlation was not found statistically significant in the female population. The correlation of the height of the specimen with the diameter of the inscribed and circumscribed circle of the canal was found to be statistically significant for the whole population.

The mean density of four individual zones for five different portions of the bone was calculated. The Average density as a whole for each of the five portions was also calculated. The results were compared for gender variability. The recorded bone density was comparable in all four zones. The pattern suggested that the average density of the bone at the distal end of the fifth metacarpal is slightly more concentrated in the posterior zone. In the proximal portion, the density is more concentrated in the anterior and medial zone for the cortex. However, in the

subchondral region of the proximal end, it is higher at the posterior zone. This pattern was less evident in female than in male population, hence it would be difficult to draw any conclusion based on a small population. In the shaft area, bone density was found to be higher than that of in the subchondral regions. We also found a correlation between weight and average density.

Table 10: Region and Zone-wise Distribution of Density in Male and Female.

Region	Average Density, Zone-wise ± SD				Total Average Density, Region-wise ± SD
	Anterior	Posterior	Lateral	Medial	
Region 1	561.2 ± 186.7	592 ± 218.1	573.9 ± 205.1	564.4 ± 230.4	573.7 ± 192.4
Region 2	1026.8 ± 333.5	1048.1 ± 337.4	1020.3 ± 327.0	1037.5 ± 340.0	1032.9 ± 324.9
Region 3	1230.5 ± 356.4	1232.7 ± 375.9	1163.8 ± 379.9	1251.7 ± 411.4	1242.0 ± 366.8
Region 4	1035.4 ± 362.0	1037.2 ± 353.1	1037.5 ± 370.9	1082.6 ± 370.5	1049.7 ± 356.4
Region 5	575.8 ± 210.4	577.9 ± 218.6	562.1 ± 218.6	545.6 ± 209.3	568.1 ± 202.6

Figure 11: Graphs plotted to represent the density distribution. Bar charts for anterior, posterior, lateral and medial zones, along with average density of the corresponding region in both male and female population.

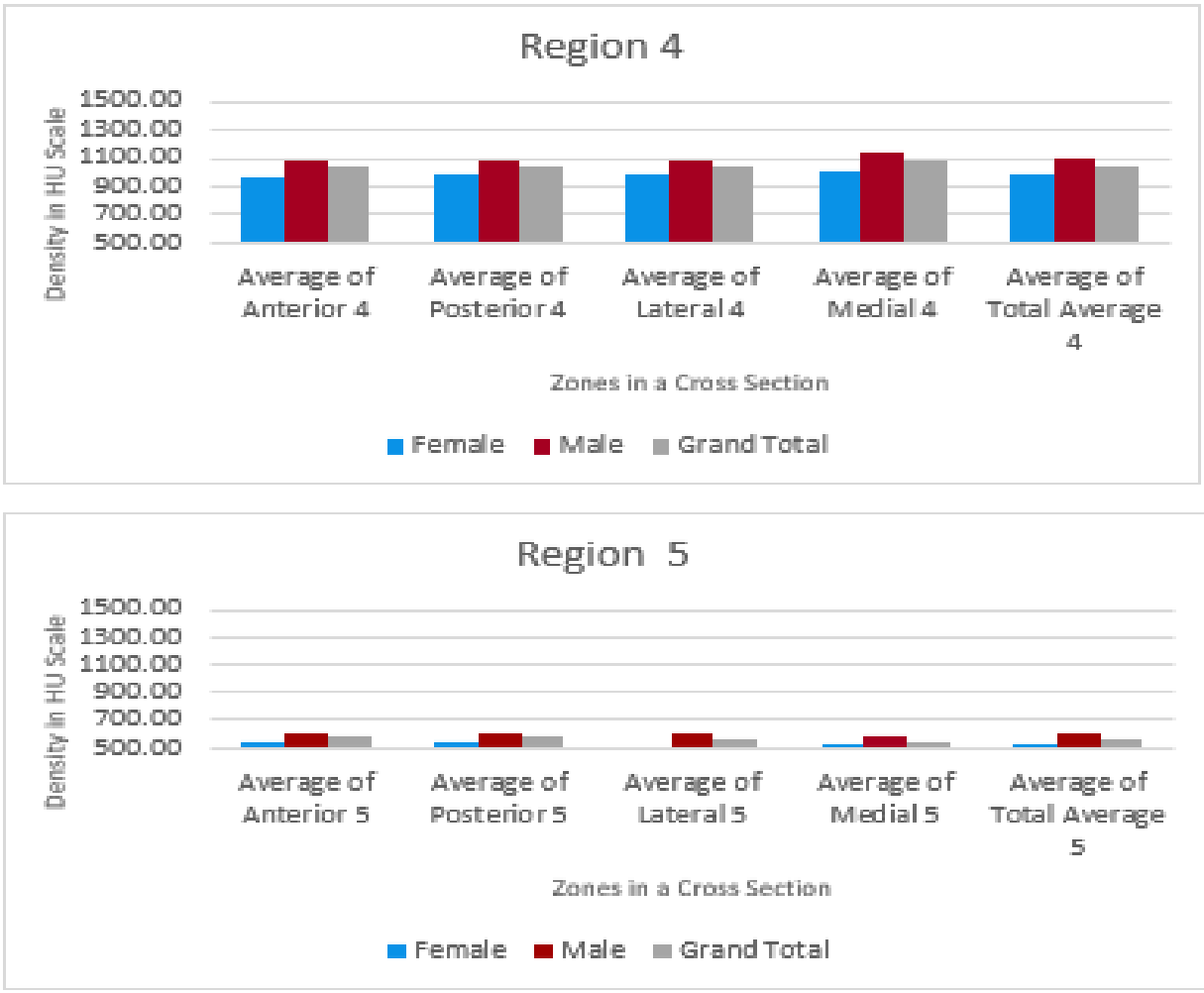

Figure 11 (continued)

The Pearson's coefficient correlation for the average density in every region with respect to the weight of the specimen was found to be statistically significant and the p-value in the order of region from head to base was observed to almost 0.05 ($p \leq 0.05$). Again, the correlation was more pronounced in the male population than the female population.

4.2 Discussions

The results of this study are in line with the previous studies in terms of density distribution and bone length. The study by John H. Musgraves and Narendra K highlighted a significant correlation between the stature of a person and the length of the bone [26]. However, the observations in this study, of the height of the specimen donor as a function of bone length suggest that the correlation is rather skewed though being statistically significant. The result of density distribution relates to the conclusion from the previous study by George Lazar et al. It states that, the dorsal cortical walls in mid-shaft are thinner than volar side. This pattern was observed while analyzing the four zones of the cortex bone. The study also suggested that the small size of the intramedullary canal at the mid-shaft and the gradual increase of diameter at the distal end is due to the thinning cortical wall at the metaphyseal area [16].

The results were more precise and apparent in the male group than in the female group. A possible explanation could be the size of the female population and its distribution. For calculation of thickness of the wall the diameter of the circumscribed circle of the canal was subtracted from the diameter of the inscribed circle of the whole bone model. The value was compared with the BMI of the specimen donor, which did not reflect a statistical significance. However, thickness correlated with bone length. We observed a correlation between the height and height percentile, with respect to the average density in the five regions. However, the correlation was not statistically significant.

This study could not meet the objective of finding a variation in measurements per the anatomical side (left and hand hands) of the fifth metacarpal bone. Observations of the left and right side of the fifth metacarpal did not show a correlation as they were collected from different

specimens and were not matching hands to make relevant comparisons. The overall information of various parameters within male and female population suggest significant variation as per the t-test.

While, the average length of the bone was compared with the previous study by Michael Rivlin et al, which was 89 ± 21 mm, this study found the average dimensions were distinctively different as 54.8 ± 4.4 mm [14]. However, it is difficult to make a comparison as the methodology of measurement used in the previous study was manual and was estimated from two different views of lateral and anterior-posterior radiographic images. The morphometry study using a 3D scan along with standardized principal component analysis reduces the human bias in estimating the dimensions and minimizes the information loss. This study also states the demography of the specimen donors along with their height percentile to provide a better picture of the population used for measurements and calculations.

Chapter 5: Conclusion and Recommendations

5.1 Implication of Results

This study is an attempt to benchmark the dimensional parameters of the fifth metacarpal bone, which can be utilized for designing the intramedullary devices. The current surgical techniques specify a screw length of 40 mm being successfully used for the treatment of fifth metacarpal bone with intramedullary devices. Most of the previous studies suggest that an IM screw with a diameter of 3 mm has worked efficiently.

The Pearson's coefficient correlation test indicates that there is a significant variation in the diameter of the inscribed and circumscribed circles of the canal model with respect to the height of the specimen donor. Hence, it suggests that the height of the patient could be a deciding factor for the selection of the screw dimensions.

The gender variability was not found statistically significant for radiodensity, which might require an effective sample size for observation. The density distribution of the cortex bone of the fifth metacarpal is comparable in four zones and therefore it is difficult to state a definitive pattern. However, the statistical analysis highlights a correlation of weight and body mass index with the density of the bone. Also, the region-wise distribution indicates that the bone density in the subchondral region of either end of the fifth metacarpal is less than that of the shaft of the bone.

The benefit of the methodology used is that the orthogonal transformation helps to provide measurement independent of the spatial placement of the specimen. The automated calculation of dimensions cancels out the chances of manual error. However, creating the bone model on the Mimics platform for the cortical region is a manual process wherein we could anticipate a certain level of observational bias. Bone modeling is dependent on the objective inclusion of the voxels that constitute the cortex region of the metacarpal bone.

The average length of the bone and diameter of the scribed circles provide a skewed set of measurement for both male and female population. The overall average of the dimensions observed is comparable with the dimensions of the existing intramedullary devices. Nevertheless, this range of measurements can supplement the analysis for the optimization of intramedullary devices. Also, the knowledge of normal dimensions and anatomic configuration can be helpful for reconstruction surgery.

5.2 Future Work and Recommendations

It would be worth investigating the variation in the right and left anatomical side with the specimens of matching hands. The data can be further diversified by adding the variable, grip strength of an individual. We expect that the hand dominance and relative activities could have a critical impact on the density distribution of the bone and its thickness.

As the morphometry and morphology of the fifth metacarpal have been stated in this study, it can be used as a foundation to carry forward the simulation of different screw size insertions in the fifth metacarpal bone. Apart from simulation, the existing devices can be verified for their strength and fit using mechanical testing methods on the cadaveric bones.

Information on the diameter of scribed circles at different planes of the fifth metacarpal can be utilized to define the dimensions of the screw implant for fractures at different anatomical planes. In addition, finite element analysis for stress and strain analysis on the fifth metacarpal bone due to IM devices is also recommended. The information on density distribution can be utilized to define the material of the bone before subjecting it to load for analysis.

References

1) Malik S, Rosenberg N. Fifth Metacarpal Fractures (Boxer's Fracture) In: StatPearls Treasure Island (FL): StatPearls Publishing; 2019 Jan.

2) Nakashian MN, Pointer L, Owens BD, Wolf JM. Incidence of metacarpal fractures in the US population. Hand (N Y). 2012;7(4):426–430.

3) Kollitz KM, Hammert WC, Vedder NB, Huang JI. Metacarpal fractures: treatment and complications. Hand (N Y). 2014;9(1):16–23.

4) Panchal-Kildare S, Malone K.; Skeletal Anatomy of the Hand: Hand Clinics, Volume 29, Issue 4, November 2013, Pages 459-471.

5) Ernest Frazer JS; Book -The Anatomy of the Human Skeleton; Publisher- J. & A. Churchill; 1920.

6) Jowett AD, Brukner PD. Fifth metacarpal stress fracture in a female softball pitcher. Clin J Sport Med. 1997;7:220-221.

7) Biswas S, Lee R, Patel A, Lifchez S. "Mirrored" Rolando's Fracture of the Base of the Fifth Metacarpal. Eplasty 2014;14:ic41. eCollection 2014.

8) Chiu YC, Tsai MT, Hsu CE, Hsu HC, Huang HL, Hsu JT. New fixation approach for transverse metacarpal neck fracture: a biomechanical study. J Orthop Surg Res. 2018;13(1):183. Published 2018 Jul 25.

9) Orbay J. Intramedullary nailing of metacarpal shaft fractures. Tech Hand Up Extrem Surg. 2005;9(2):69–73.

10) Galal S, Safwat W. Transverse pinning versus intramedullary pinning in fifth metacarpal's neck fractures: A randomized controlled study with patient-reported outcome. J Clin Orthop Trauma. 2017;8(4):339–343.

11) Tobert DG, Klausmeyer M, Mudgal CS. Intramedullary Fixation of Metacarpal Fractures Using Headless Compression Screws. J Hand Microsurg. 2016;8(3):134–139.

12) Doarn, M. C., Nydick, J. A., Williams, B. D., & Garcia, M. J. (2014). Retrograde Headless Intramedullary Screw Fixation for Displaced Fifth Metacarpal Neck and Shaft Fractures: Short Term Results. Hand, 10(2), 314-318.

13) Rolison CJ, Smoot MK. Hand Pain in a Golfer: A Case Report of a Metacarpal Stress Injury and a Review of the Literature Regarding Return to Play in Grip Athletes. Sports Health. 2017;9(1):84–86.

14) Rivlin M, Kim N, Lutsky KF, Beredjiklian PK. Measurement of the radiographic anatomy of the small and ring metacarpals using computerized tomographic scans. Hand (N Y). 2015;10(4):756–761.

15) ten Berg, Paul W L, Mudgal, Chaitanya S, Leibman, Matthew I, Belsky, Mark R, Ruchelsman David E. Quantitative 3-Dimensional CT Analyses of Intramedullary Headless Screw Fixation for Metacarpal Neck Fractures; The Journal of Hand Surgery; Volume 38, Issue 2, February 2013, Pages 322-330.e2.

16) Lazar G, Frances P. Schulter-Ellis. Intramedullary structure of human metacarpals; THE JOURNAL OF HAND SURGERY; 1980 American Society for Surgery of the Hand.

17) Llorente I; Merino L, Escolano E, Quintanilla DM, García-Vadillo JA; González-Álvaro I, Castañeda S. Reproducibility of Metacarpal Bone Mineral Density Measurements Obtained by Dual-Energy X-Ray Absorptiometry in Healthy Volunteers and Patients With Early Arthritis; Journal of Clinical Densitometry; pub: 27 February 2019.

18) Douglass N, Yao J. Nuts and Bolts; Dimensions of Commonly Utilized Screws in Upper Extremity Surgery; J Hand Surg Am. 2015 Feb;40(2):368-82.

19) Randall ME. Practical Biomechanics: Intramedullary Fixation Devices; Techniques in Orthopaedics: January 1998.

20) Tobert DG, Klausmeyer M, Mudgal CS. Intramedullary Fixation of Metacarpal Fractures Using Headless Compression Screws. J Hand Microsurg. 2016;8(3):134–139.

21) Boulton CL, Salzler M, Mudgal CS; Intramedullary Cannulated Headless Screw Fixation of a Comminuted Subcapital Metacarpal Fracture: Case Report; Journal of Hand Surgery, Volume 35, Issue 8, 1260 – 1263.

22) Vaux JJ, Hugate RR, Hills JW, Grzybowski RF, Funk CK; Morphometrics of the human thumb metacarpal bone: interest for developing an osseointegrated prosthesis; Surg Radiol Anat (2016) 38:127–133.

23) Alidousti H, Giles JW, Emery RJH, Jeffers J. Spatial mapping of humeral head bone density. J Shoulder Elbow Surg. 2017;26(9):1653–1661.

24) Simon P, Gupta A, Hussey M, Pappou I, Santoni BG, Inoue N, Frankle MA. "The Relationship Between the Subchondral Bone Density Distribution and Glenoid Depth: An In Vivo Study of Male Total Shoulder Arthroplasty Patients." J. of Shoulder & Elbow Surg. 2015 Mar; 24(3):416-24.

25) Aira JR, Simon P, Gutiérrez S, Santoni BG, Frankle MA. "Morphometry of the human clavicle and intramedullary canal: A 3D, geometry-based quantification." J Orthop Res. 2017 Oct;35(10):2191-2202.

26) Musgrave JH, Harneja NK. The estimation of adult stature from metacarpal bone length. Am. J. Phys. Anthropol., 8 (1) (1978), pp. 113-119.

27) Pogliacomi F, Mijno E, Pedrazzini A, et al. Fifth metacarpal neck fractures: fixation with antegrade locked flexible intramedullary nailing. *Acta Biomed*. 2017;88(1):57–64. Published 2017 Apr 28.

28) Yang, Y., Scheker, L. R., & Kumar, K. K. (2015). Arthroplasty for fifth carpometacarpal joint arthritis. Journal of wrist surgery, 4(2), 110–114.

29) Lee S, Chung CK, Oh SH, Park SB. Correlation between Bone Mineral Density Measured by Dual-Energy X-Ray Absorptiometry and Hounsfield Units Measured by Diagnostic CT in Lumbar Spine. J Korean Neurosurg Soc. 2013;54(5):384–389.

30) Clark EM, Ness AR, Bishop NJ, Tobias JH. Association between bone mass and fractures in children: a prospective cohort study. J Bone Miner Res. 2006;21(9):1489–1495.

31) Ramakrishna S, Huang ZM, Compressive Structural Integrity, Vol9: Bioengineering, eds Teoh SH and Mai YW (Elsevier Science Publisher, UK 2003).

Appendix A: Table of Results

Table A1: Results of Minimum Values of Scribed Circles.

Specimen Number	Articular Side	Gender	Length of the bone	Length of bone Categorized	Height in cm	Weight in Kg	Diameter CIC	plane reference of the value CIC	Diameter CCC	plane reference of the value CCC	Diameter OIC	plane reference of the value OIC	Diameter OCC	plane reference of the value OCC
GL1706803	Right	Female	51.87	51-54	152	48	3.22	23	5.36	22	7.28	21	9.91	21
GL1810231	Left	Male	58.94	57-60	188	61	4.43	23	4.02	17	5.13	26	7.14	23
GL1706524	Left	Male	58.66	57-60	180	68	4.25	16	5.64	19	6.51	19	8.77	26
GL1809034	Right	Female	50.62	48-51	137	54	2.98	28	4.36	26	6.47	23	7.72	25
GL1707366	Left	Female	48.67	48-51	152	57	4.06	18	3.88	26	6.20	22	7.56	25
GL1707011	Right	Male	58.11	57-60	168	44	2.67	31	3.69	28	5.95	24	7.92	25
GL1809025	Left	Male	52.12	51-54	170	61	5.01	22	6.32	28	6.27	18	10.55	23
GL1810619	Right	Male	60.34	60-63	183	91	3.15	22	3.99	23	7.48	22	9.88	24
GL1706730	Left	Male	58.69	57-60	178	113	3.54	22	4.99	17	7.34	27	9.46	19
GL1810671	Right	Male	57.00	54-57	170	52	3.81	24	4.61	24	7.93	18	9.60	25
GL1707122	Left	Male	57.32	57-60	173	75	3.06	24	4.00	17	6.45	20	8.26	25
GL1707136	Right	Female	54.26	54-57	168	61	3.47	27	3.67	24	5.42	15	7.92	18
GL1810218	Left	Male	60.62	60-63	178	91	3.77	27	3.82	24	7.49	12	8.79	22
GL1706741	Right	Male	57.17	57-60	183	82	2.28	23	2.91	18	6.92	33	7.97	23
GL1810540	Right	Female	46.61	45-48	163	68	2.74	34	2.56	26	5.36	32	6.69	26
GL1810414	Left	Female	50.93	48-51	165	54	3.07	28	3.78	24	5.18	14	7.24	23
GL1810188	Left	Female	50.91	48-51	165	59	2.45	29	3.74	23	4.42	23	7.46	23

Table A1 (continued)

Specimen Number	Articular Side	Gender	Length of the bone	Length of bone Categorized	Height in cm	Weight in Kg	Diameter CIC	plane reference of the value CIC	Diameter CCC	plane reference of the value CCC	Diameter OIC	plane reference of the value OIC	Diameter OCC	plane reference of the value OCC
CI81372	Right	Female	51.84	51-54	155	68	3.15	37	4.08	27	5.93	29	7.15	28
F182611	Left	Male	58.96	57-60	168	73	4.48	28	4.70	17	7.58	23	9.91	21
S190261	Left	Male	58.42	57-60	170	89	4.09	19	5.44	19	7.05	22	8.67	26
I190129	Right	Female	50.17	48-51	155	37	3.43	30	4.38	24	6.71	25	7.45	28
F182566	Left	Female	48.85	48-51	150	66	3.07	24	3.51	26	5.77	22	7.52	25
S182714	Right	Male	57.96	57-60	183	89	2.67	16	3.60	21	5.05	16	7.70	24
F190645	Right	Male	59.72	57-60	178	67	2.77	26	4.05	29	6.33	13	9.09	30
F1901070	Left	Male	59.59	57-60	178	68	3.15	23	3.99	22	7.48	23	9.88	24
GL1504015	Right	Male	56.60	54-57	170	70	4.03	25	4.42	25	8.52	26	10.90	24
C190245	Right	Female	52.92	51-54	157	49	2.59	22	2.81	22	7.23	25	9.26	21
GL1706904	Right	Male	60.44	60-63	185	71	3.52	26	3.45	27	8.02	17	9.67	32
S182705	Right	Female	49.36	48-51	147	45	3.53	21	4.84	21	4.72	29	8.06	22
S190235	Right	Female	46.54	45-48	163	68	1.92	30	2.87	26	5.18	17	7.02	24
C181847	Right	Male	58.66	57-60	183	70	1.85	27	3.42	33	5.29	35	9.45	31
I181079	Right	Female	52.33	51-54	175	44	3.69	17	4.27	19	6.07	15	7.40	24
C190111	Right	Male	55.29	54-57	173	104	4.46	23	5.11	24	7.54	28	9.06	24
C181432	Left	Male	61.98	60-63	188	54	2.64	27	3.36	28	7.86	29	9.47	20
S190655	Right	Male	51.69	51-54	175	68	2.98	22	2.92	21	6.60	16	8.07	27
F182481	Right	Female	51.87	51-54	170	80	2.28	26	2.89	25	6.33	35	8.62	32
GL1707410	Right	Male	56.12	54-57	180	113	3.70	26	6.36	28	8.33	32	10.57	33
GL1810754	Right	Female	50.68	48-51	175	54	2.12	24	3.18	23	6.16	27	7.07	22

Table A2: Results of Density Distribution, Part 1.

Specimen Number	Anterior 1	Posterior 1	Lateral 1	Medial 1	TA 1	Anterior 2	Posterior 2	Lateral 2	Medial 2	TA 2	Anterior 3	Posterior 3	Lateral 3	Medial 3	TA 3
GL1706803	436.26	370.02	276.06	412.29	379.32	812.72	864.31	660.50	824.25	784.99	1064.78	1183.84	1000.59	1023.23	1063.49
GL1810231	590.44	493.97	459.90	580.52	516.86	1166.38	1341.96	1132.59	1294.45	1234.41	1403.62	1437.46	1474.27	1510.03	1456.13
GL1706524	548.15	688.31	585.26	440.82	574.46	1050.44	1405.43	1099.91	911.99	1116.91	1433.61	1523.42	1505.07	1317.80	1425.27
GL1809034	373.78	426.12	505.39	371.76	427.35	923.19	945.50	974.88	925.57	937.79	1052.63	1252.15	1103.95	1266.99	1163.14
GL1707366	669.70	615.46	745.71	592.78	664.15	1202.11	1220.40	1357.60	1283.01	1255.26	1310.36	1358.28	1237.12	1454.94	1371.66
GL1707011	481.10	496.95	573.24	425.10	499.60	1165.63	1159.51	1086.90	1133.89	1143.98	1400.60	1280.26	1246.56	1412.52	1372.67
GL1809025	585.39	603.74	739.19	586.88	635.91	956.88	1061.75	1146.86	1067.70	1057.37	1359.38	1236.38	1300.27	1539.27	1359.87
GL1810619	639.98	709.87	675.99	549.77	658.88	1213.53	1267.45	1290.69	1336.78	1265.00	1467.32	1430.99	1357.37	1580.44	1493.51
GL1706730	912.67	850.26	883.06	643.31	829.59	1516.35	1335.95	1316.85	1404.45	1396.02	1581.59	1595.88	1423.36	1607.72	1583.95
GL1810671	650.78	859.58	798.42	1042.36	795.24	1114.12	1249.14	1101.86	1044.15	1120.51	1128.12	1547.45	980.09	1705.95	1431.03
GL1707122	597.27	578.81	666.86	493.10	594.80	995.07	1215.54	1316.79	1162.38	1161.58	1500.50	1465.32	1313.44	1506.43	1472.35
GL1707136	643.60	596.66	500.04	561.68	574.20	1163.10	1025.56	982.46	1023.95	1057.37	1389.68	1291.20	1453.11	1296.51	1335.88
GL1810218	662.98	837.26	604.59	601.30	684.19	1141.42	1449.77	1252.53	1274.41	1287.67	1549.54	1577.23	1468.14	1465.51	1514.32
GL1706741	1051.03	909.65	1048.87	774.57	953.08	1729.92	1476.79	1703.38	1587.41	1640.59	1844.48	1750.91	1835.49	1851.96	1836.56
GL1810540	705.75	861.05	732.31	927.92	794.29	1405.67	1388.93	1226.16	1589.71	1418.37	1428.72	1674.08	1547.80	1771.79	1678.65
GL1810414	532.68	625.78	604.88	571.99	579.09	938.11	863.04	1020.89	854.52	923.53	1082.10	1142.63	1076.44	887.33	1064.75
GL1810188	499.99	595.43	533.92	556.72	543.58	811.59	765.97	861.09	787.95	809.08	926.12	1061.91	969.66	830.31	967.77
GL1707410	902.55	1134.27	982.50	1198.46	1036.76	1633.82	1451.84	1353.14	1569.90	1500.56	1835.20	1731.11	1645.89	1803.53	1765.74
GL1810754	613.48	763.46	672.09	646.27	682.27	1347.77	1450.50	1251.13	1349.25	1348.39	1728.71	1462.16	1549.19	1676.26	1657.71

Table A2 (continued)

Specimen Number	Anterior 1	Posterior 1	Lateral 1	Medial 1	TA 1	Anterior 2	Posterior 2	Lateral 2	Medial 2	TA 2	Anterior 3	Posterior 3	Lateral 3	Medial 3	TA 3
CI81372	463.96	380.82	296.01	457.10	405.34	804.42	913.57	705.83	864.30	814.42	1077.30	1138.08	1027.47	1093.23	1074.27
F182611	574.05	478.57	453.19	582.49	508.19	1177.51	1357.49	1100.88	1356.21	1251.99	1371.82	1386.47	1390.32	1480.89	1416.80
S190261	690.24	552.52	549.50	547.42	580.38	1218.95	1174.27	1305.35	982.14	1162.02	1525.71	1524.62	1595.73	1447.96	1510.08
I190129	427.24	468.22	570.72	411.78	477.56	1053.58	1103.49	1061.46	1070.55	1069.34	1139.23	1332.60	1261.91	1310.69	1246.73
F182566	654.64	605.44	729.77	593.95	651.45	1202.61	1260.70	1361.71	1308.36	1276.18	1430.00	1380.25	1359.60	1454.74	1414.58
S182714	488.98	526.08	591.68	441.98	518.69	1281.65	1304.52	1207.63	1230.01	1262.69	1481.97	1408.28	1422.64	1464.40	1459.46
F190645	323.47	264.10	346.03	228.49	299.26	455.12	412.44	439.91	467.23	443.26	512.19	549.53	333.87	552.98	525.05
F1901070	366.60	398.62	348.33	312.44	360.69	456.97	514.52	527.43	488.77	493.77	689.92	689.28	574.85	710.54	684.13
GL1504015	441.48	403.36	395.79	424.98	415.87	622.77	806.85	691.60	731.31	698.71	962.63	842.58	953.04	716.04	912.08
C190245	650.78	859.58	798.42	1042.36	795.24	1114.12	1249.14	1101.86	1044.15	1120.51	1128.12	1547.45	980.09	1705.95	1431.03
GL1706904	407.34	476.92	470.88	355.62	442.08	922.02	720.13	710.82	692.67	792.06	1039.77	692.37	672.02	801.48	869.80
S182705	347.55	296.80	380.25	239.78	326.32	768.46	546.93	811.61	677.16	693.16	998.25	793.73	769.79	772.83	848.65
S190235	628.16	678.64	497.67	730.50	646.86	1075.27	1163.96	1192.87	1343.78	1182.40	1368.38	1510.40	1578.44	1308.53	1501.10
C181847	976.65	1088.71	879.03	874.86	951.97	1519.45	1382.54	1456.17	1411.60	1430.92	1522.02	1541.31	1159.24	1483.74	1488.71
I181079	286.43	342.97	272.07	314.41	299.10	624.86	557.26	546.60	658.79	597.26	1060.15	852.77	856.79	888.69	896.73
C190111	544.36	604.29	714.58	824.84	668.94	1004.11	988.05	1048.71	1255.20	1085.14	1416.35	1286.67	1391.38	1423.47	1359.41
C181432	359.61	431.64	421.97	464.86	426.31	708.93	703.71	687.42	713.34	704.18	711.56	550.43	628.34	711.69	683.32
S190655	264.90	233.23	231.02	200.59	238.36	362.06	360.67	304.10	354.91	350.90	368.11	442.30	285.39	443.67	410.81
F182481	331.56	386.89	272.66	421.99	363.74	357.22	369.56	372.81	346.96	363.50	468.34	369.33	496.07	284.73	450.24

Table A3: Results of Density Distribution, Part 2.

Specimen Number	Articular Side	Gender	Length of the bone	Length of bone Categorized	Height in cm	Weight in Kg	Anterior 4	Posterior 4	Lateral 4	Medial 4	TA 4	Anterior 5	Posterior 5	Lateral 5	Medial 5	TA 5
GL1706803	Right	Female	51.87	51-54	152	48	636.51	790.43	827.14	864.19	759.20	321.49	301.04	198.83	345.05	301.16
GL1810231	Left	Male	58.94	57-60	188	61	1340.22	1188.86	1372.79	1179.15	1261.48	626.39	532.83	625.56	493.84	576.81
GL1706524	Left	Male	58.66	57-60	180	68	1170.49	970.76	885.12	1029.60	1020.98	537.21	435.92	575.78	426.91	505.30
GL1809034	Right	Female	50.62	48-51	137	54	772.39	1004.87	843.49	874.01	863.45	520.72	390.78	444.85	445.53	442.97
GL1707366	Left	Female	48.67	48-51	152	57	1200.03	996.31	882.26	1205.30	1077.21	663.94	663.75	538.17	602.45	608.64
GL1707011	Right	Male	58.11	57-60	168	44	1081.40	1267.13	1115.03	1198.35	1161.97	527.81	548.34	498.12	446.75	508.17
GL1809025	Left	Male	52.12	51-54	170	61	1017.54	1110.02	969.20	1270.14	1112.28	614.23	823.54	647.64	760.65	686.53
GL1810619	Right	Male	60.34	60-63	183	91	1356.06	1257.47	1352.96	1427.20	1358.41	809.44	709.04	694.75	843.34	754.67
GL1706730	Left	Male	58.69	57-60	178	113	1401.47	1485.84	1433.66	1540.63	1471.38	903.02	1066.23	939.29	784.35	938.38
GL1810671	Right	Male	57.00	54-57	170	52	1457.18	1521.47	1614.96	1640.69	1567.31	795.25	744.10	929.07	822.29	832.37
GL1707122	Left	Male	57.32	57-60	173	75	1308.82	1140.74	1079.74	1323.05	1217.57	595.15	687.93	530.06	655.65	604.95
GL1707136	Right	Female	54.26	54-57	168	61	1037.97	1156.69	1034.19	1215.73	1118.86	524.45	636.49	555.61	470.90	560.83
GL1810218	Left	Male	60.62	60-63	178	91	1197.72	1079.14	1255.86	1261.84	1199.29	633.86	565.33	726.51	476.94	614.78
GL1706741	Right	Male	57.17	57-60	183	82	1684.42	1736.49	1671.69	1806.92	1730.78	1164.52	780.43	797.24	1116.52	936.17
GL1810540	Right	Female	46.61	45-48	163	68	1379.88	1378.89	1472.76	1517.94	1428.47	787.53	804.62	807.64	687.97	780.69
GL1810414	Left	Female	50.93	48-51	165	54	806.39	902.24	869.84	799.54	854.37	512.53	533.72	425.36	490.28	496.98
GL1810188	Left	Female	50.91	48-51	165	59	768.68	915.76	870.57	807.26	851.85	493.28	539.19	398.52	505.98	490.14
GL1707410	Right	Male	56.12	54-57	180	113	1649.44	1715.52	1619.83	1705.75	1678.69	1044.86	1239.87	1137.72	994.85	1108.37

Table A3 (continued)

Specimen Number	Articular Side	Gender	Length of the bone	Length of bone Categorized	Height in cm	Weight in Kg	Anterior 4	Posterior 4	Lateral 4	Medial 4	TA 4	Anterior 5	Posterior 5	Lateral 5	Medial 5	TA 5
GL1810754	Right	Female	50.68	48-51	175	54	1617.77	1062.31	1487.82	1319.66	1383.25	775.96	659.48	617.34	718.61	686.24
Cl81372	Right	Female	51.84	51-54	155	68	647.16	823.57	866.32	873.47	782.25	326.86	312.69	230.09	359.15	314.83
F182611	Left	Male	58.96	57-60	168	73	1283.29	1101.85	1323.15	1141.95	1202.44	593.07	503.42	586.22	467.52	543.42
S190261	Left	Male	58.42	57-60	170	89	1031.39	1029.45	918.08	1093.75	1022.19	368.92	516.92	562.74	526.53	507.45
I190129	Right	Female	50.17	48-51	155	37	809.46	1030.68	890.59	902.06	899.88	549.26	445.64	476.27	488.13	484.39
F182566	Left	Female	48.85	48-51	150	66	1219.35	998.59	972.81	1174.66	1093.09	644.07	705.88	582.26	621.82	632.56
S182714	Right	Male	57.96	57-60	183	89	1092.23	1279.53	1167.59	1234.65	1189.42	533.88	554.14	501.57	448.19	512.89
F190645	Right	Male	59.72	57-60	178	67	398.49	417.58	423.42	446.80	419.68	296.33	286.80	294.97	260.11	288.17
F1901070	Left	Male	59.59	57-60	178	68	642.45	574.55	623.58	606.20	610.20	377.41	385.26	432.45	300.93	384.71
GL1504015	Right	Male	56.60	54-57	170	70	741.46	628.57	675.95	774.10	701.74	417.58	520.37	394.71	427.76	454.29
C190245	Right	Female	52.92	51-54	157	49	1457.18	1521.47	1614.96	1640.69	1567.31	795.25	744.10	929.07	822.29	832.37
GL1706904	Right	Male	60.44	60-63	185	71	863.57	617.59	666.69	789.14	756.47	392.12	391.17	459.56	449.64	424.57
S182705	Right	Female	49.36	48-51	147	45	616.84	666.75	587.24	589.13	615.55	446.66	409.60	394.98	351.07	401.67
S190235	Right	Female	46.54	45-48	163	68	1408.12	1364.18	1414.27	1219.29	1359.00	595.85	662.12	633.16	540.11	600.59
C181847	Right	Male	58.66	57-60	183	70	1123.49	1440.19	1389.48	1411.51	1323.87	778.93	944.32	868.96	769.36	848.08
I181079	Right	Female	52.33	51-54	175	44	713.16	780.54	678.86	747.65	738.34	348.43	367.52	384.15	239.87	342.80
C190111	Right	Male	55.29	54-57	173	104	956.10	1076.29	1159.64	1028.93	1057.40	614.93	527.44	641.81	575.66	598.51
C181432	Left	Male	61.98	60-63	188	54	708.93	703.71	687.42	713.34	704.18	359.61	431.64	421.97	464.86	426.31
S190655	Right	Male	51.69	51-54	175	68	279.36	294.16	252.56	306.25	287.15	187.06	185.63	172.77	164.03	177.44
F182481	Right	Female	51.87	51-54	170	80	470.32	382.00	454.78	458.94	442.53	401.99	401.35	302.50	364.90	377.82

Appendix B: Statistical Analysis from SAS

Amrita data analysis - more focused for thesis

(by gender)

The CORR Procedure

Gender=Female

7 Variables:	Ht_perc Ht_Inch BLength DiamCIC DiamCCC DiamOCC DiamOIC

Simple Statistics

Variable	N	Mean	Std Dev	Sum	Minimum	Maximum
Ht_perc	16	21.37500	16.33350	342.00000	0	47.00000
Ht_Inch	16	62.75000	4.12311	1004	54.00000	69.00000
BLength	16	50.52688	2.12249	808.43000	46.54000	54.26000
DiamCIC	16	2.98563	0.59786	47.77000	1.92000	4.06000
DiamCCC	16	3.76125	0.78090	60.18000	2.56000	5.36000
DiamOCC	16	7.75313	0.85452	124.05000	6.69000	9.91000
DiamOIC	16	5.90188	0.82402	94.43000	4.42000	7.28000

Pearson Correlation Coefficients, N = 16
Prob > |r| under H0: Rho=0

	Ht_perc	Ht_Inch	BLength	DiamCIC	DiamCCC	DiamOCC	DiamOIC
Ht_perc	1.00000	-0.23511 0.3807	-0.28153 0.2908	0.07384 0.7858	-0.17545 0.5157	0.00182 0.9947	0.15132 0.5759
Ht_Inch	-0.23511 0.3807	1.00000	0.23553 0.3799	-0.33285 0.2078	-0.45853 0.0740	-0.21850 0.4162	-0.18744 0.4870
BLength	-0.28153 0.2908	0.23553 0.3799	1.00000	0.19389 0.4718	0.26715 0.3172	0.51539 0.0410	0.34832 0.1861
DiamCIC	0.07384 0.7858	-0.33285 0.2078	0.19389 0.4718	1.00000	0.63665 0.0080	0.07613 0.7793	0.11077 0.6830
DiamCCC	-0.17545 0.5157	-0.45853 0.0740	0.26715 0.3172	0.63665 0.0080	1.00000	0.33528 0.2043	0.15555 0.5651
DiamOCC	0.00182 0.9947	-0.21850 0.4162	0.51539 0.0410	0.07613 0.7793	0.33528 0.2043	1.00000	0.59350 0.0154
DiamOIC	0.15132 0.5759	-0.18744 0.4870	0.34832 0.1861	0.11077 0.6830	0.15555 0.5651	0.59350 0.0154	1.00000

Figure B1: Data analysis from SAS for female population.

Amrita data analysis - more focused for thesis

(by gender)

The CORR Procedure

Gender=Male

7 Variables:	Ht_perc Ht_Inch BLength DiamCIC DiamCCC DiamOCC DiamOIC

Simple Statistics						
Variable	N	Mean	Std Dev	Sum	Minimum	Maximum
Ht_perc	22	19.00000	14.63525	418.00000	1.00000	46.00000
Ht_Inch	22	69.81818	2.53802	1536	66.00000	74.00000
BLength	22	57.92727	2.50929	1274	51.69000	61.98000
DiamCIC	22	3.46864	0.81586	76.31000	1.85000	5.01000
DiamCCC	22	4.30955	0.98929	94.81000	2.91000	6.36000
DiamOCC	22	9.12636	0.99890	200.78000	7.14000	10.90000
DiamOIC	22	6.96000	1.00363	153.12000	5.05000	8.52000

Pearson Correlation Coefficients, N = 22 Prob > |r| under H0: Rho=0							
	Ht_perc	Ht_Inch	BLength	DiamCIC	DiamCCC	DiamOCC	DiamOIC
Ht_perc	1.00000	-0.77817 <.0001	-0.38799 0.0744	0.45632 0.0328	0.32893 0.1350	0.08918 0.6931	0.27975 0.2073
Ht_Inch	-0.77817 <.0001	1.00000	0.46462 0.0294	-0.38809 0.0743	-0.38162 0.0797	-0.22341 0.3176	-0.18377 0.4130
BLength	-0.38799 0.0744	0.46462 0.0294	1.00000	-0.28436 0.1996	-0.30162 0.1725	-0.04006 0.8595	0.10713 0.6351
DiamCIC	0.45632 0.0328	-0.38809 0.0743	-0.28436 0.1996	1.00000	0.73093 <.0001	0.29069 0.1894	0.27209 0.2206
DiamCCC	0.32893 0.1350	-0.38162 0.0797	-0.30162 0.1725	0.73093 <.0001	1.00000	0.47948 0.0239	0.23357 0.2955
DiamOCC	0.08918 0.6931	-0.22341 0.3176	-0.04006 0.8595	0.29069 0.1894	0.47948 0.0239	1.00000	0.68089 0.0005
DiamOIC	0.27975 0.2073	-0.18377 0.4130	0.10713 0.6351	0.27209 0.2206	0.23357 0.2955	0.68089 0.0005	1.00000

Figure B2: Data analysis from SAS for male population.

Amrita data analysis - more focused for thesis

(by gender)

The CORR Procedure

Gender=Female

9 Variables:	Ht_inch Wt BMI BLength Av1 Av2 Av3 Av4 Av5

Simple Statistics

Variable	N	Mean	Std Dev	Sum	Minimum	Maximum
Ht_inch	16	62.75000	4.12311	1004	54.00000	69.00000
Wt	16	125.81250	24.48460	2013	81.00000	176.00000
BMI	16	22.62913	4.70258	362.06604	14.47049	29.28325
BLength	16	50.52688	2.12249	808.43000	46.54000	54.26000
Av1	16	538.11625	160.67740	8610	299.10000	795.24000
Av2	16	978.22188	291.48645	15652	363.50000	1418
Av3	16	1198	322.93581	19166	450.24000	1679
Av4	16	989.66313	317.54272	15835	442.53000	1567
Av5	16	522.16750	160.41808	8355	301.16000	832.37000

Pearson Correlation Coefficients, N = 16
Prob > |r| under H0: Rho=0

	Ht_inch	Wt	BMI	BLength	Av1	Av2	Av3	Av4	Av5
Ht_inch	1.00000	0.19564 0.4678	-0.44866 0.0813	0.23553 0.3799	0.11369 0.6751	-0.09655 0.7221	-0.02887 0.9155	0.11981 0.6585	0.11356 0.6754
Wt	0.19564 0.4678	1.00000	0.77996 0.0004	-0.21359 0.4270	0.21406 0.4260	0.00097 0.9971	-0.04203 0.8772	0.03818 0.8884	0.11797 0.6635
BMI	-0.44866 0.0813	0.77996 0.0004	1.00000	-0.33203 0.2090	0.11871 0.6615	0.07973 0.7691	0.00569 0.9833	-0.02645 0.9225	0.03361 0.9017
BLength	0.23553 0.3799	-0.21359 0.4270	-0.33203 0.2090	1.00000	-0.36452 0.1651	-0.49968 0.0487	-0.41624 0.1088	-0.29899 0.2606	-0.33702 0.2018
Av1	0.11369 0.6751	0.21406 0.4260	0.11871 0.6615	-0.36452 0.1651	1.00000	0.85875 <.0001	0.82492 <.0001	0.91101 <.0001	0.95443 <.0001
Av2	-0.09655 0.7221	0.00097 0.9971	0.07973 0.7691	-0.49968 0.0487	0.85875 <.0001	1.00000	0.97218 <.0001	0.86906 <.0001	0.81155 0.0001
Av3	-0.02887 0.9155	-0.04203 0.8772	0.00569 0.9833	-0.41624 0.1088	0.82492 <.0001	0.97218 <.0001	1.00000	0.92043 <.0001	0.78641 0.0003
Av4	0.11981 0.6585	0.03818 0.8884	-0.02645 0.9225	-0.29899 0.2606	0.91101 <.0001	0.86906 <.0001	0.92043 <.0001	1.00000	0.90884 <.0001
Av5	0.11356 0.6754	0.11797 0.6635	0.03361 0.9017	-0.33702 0.2018	0.95443 <.0001	0.81155 0.0001	0.78641 0.0003	0.90884 <.0001	1.00000

Figure B3: Density Data Analysis from SAS for female population.

Amrita data analysis - more focused for thesis

(by gender)

The CORR Procedure

Gender=Male

9 Variables:	Ht_inch Wt BMI BLength Av1 Av2 Av3 Av4 Av5

Simple Statistics

Variable	N	Mean	Std Dev	Sum	Minimum	Maximum
Ht_inch	22	69.81818	2.53802	1536	66.00000	74.00000
Wt	22	167.86364	41.07519	3693	96.00000	250.00000
BMI	22	24.24147	5.96436	533.31244	15.40541	35.86735
BLength	22	57.92727	2.50929	1274	51.69000	61.98000
Av1	22	599.55045	212.39403	13190	238.36000	1037
Av2	22	1073	348.35505	23600	350.90000	1641
Av3	22	1274	399.91701	28031	410.81000	1837
Av4	22	1093	383.47513	24055	287.15000	1731
Av5	22	601.47000	226.22285	13232	177.44000	1108

Pearson Correlation Coefficients, N = 22
Prob > |r| under H0: Rho=0

	Ht_inch	Wt	BMI	BLength	Av1	Av2	Av3	Av4	Av5
Ht_inch	1.00000	0.11760 0.6022	-0.14402 0.5225	0.46462 0.0294	0.10551 0.6403	0.09120 0.6865	-0.04035 0.8585	0.04428 0.8449	0.09759 0.6657
Wt	0.11760 0.6022	1.00000	0.96382 <.0001	-0.03398 0.8807	0.48730 0.0214	0.43938 0.0408	0.43894 0.0410	0.36874 0.0913	0.48568 0.0219
BMI	-0.14402 0.5225	0.96382 <.0001	1.00000	-0.14837 0.5099	0.43832 0.0413	0.39751 0.0669	0.43178 0.0448	0.33268 0.1303	0.43480 0.0432
BLength	0.46462 0.0294	-0.03398 0.8807	-0.14837 0.5099	1.00000	-0.05266 0.8160	0.07953 0.7250	-0.00093 0.9967	0.03145 0.8895	-0.04083 0.8568
Av1	0.10551 0.6403	0.48730 0.0214	0.43832 0.0413	-0.05266 0.8160	1.00000	0.86047 <.0001	0.83072 <.0001	0.89481 <.0001	0.96621 <.0001
Av2	0.09120 0.6865	0.43938 0.0408	0.39751 0.0669	0.07953 0.7250	0.86047 <.0001	1.00000	0.97529 <.0001	0.94619 <.0001	0.84235 <.0001
Av3	-0.04035 0.8585	0.43894 0.0410	0.43178 0.0448	-0.00093 0.9967	0.83072 <.0001	0.97529 <.0001	1.00000	0.94103 <.0001	0.81971 <.0001
Av4	0.04428 0.8449	0.36874 0.0913	0.33268 0.1303	0.03145 0.8895	0.89481 <.0001	0.94619 <.0001	0.94103 <.0001	1.00000	0.92173 <.0001
Av5	0.09759 0.6657	0.48568 0.0219	0.43480 0.0432	-0.04083 0.8568	0.96621 <.0001	0.84235 <.0001	0.81971 <.0001	0.92173 <.0001	1.00000

Figure B4: Density data analysis from SAS for male population.

Amrita data analysis - more focused for thesis

(all data combined)

The CORR Procedure

9 Variables:	Ht_inch Wt BMI BLength Av1 Av2 Av3 Av4 Av5

Simple Statistics

Variable	N	Mean	Std Dev	Sum	Minimum	Maximum
Ht_inch	38	66.84211	4.80161	2540	54.00000	74.00000
Wt	38	150.15789	40.53795	5706	81.00000	250.00000
BMI	38	23.56259	5.45953	895.37849	14.47049	35.86735
BLength	38	54.81132	4.37161	2083	46.54000	61.98000
Av1	38	573.68342	192.39281	21800	238.36000	1037
Av2	38	1033	324.89467	39252	350.90000	1641
Av3	38	1242	366.75205	47197	410.81000	1837
Av4	38	1050	356.42020	39889	287.15000	1731
Av5	38	568.07947	202.61644	21587	177.44000	1108

Pearson Correlation Coefficients, N = 38
Prob > |r| under H0: Rho=0

	Ht_inch	Wt	BMI	BLength	Av1	Av2	Av3	Av4	Av5
Ht_inch	1.00000	0.45917 0.0037	-0.07290 0.6636	0.74368 <.0001	0.18567 0.2644	0.10639 0.5249	0.05456 0.7449	0.15872 0.3412	0.20823 0.2096
Wt	0.45917 0.0037	1.00000	0.84674 <.0001	0.40302 0.0121	0.43608 0.0062	0.34689 0.0330	0.32018 0.0500	0.31207 0.0565	0.43637 0.0062
BMI	-0.07290 0.6636	0.84674 <.0001	1.00000	0.01607 0.9237	0.35826 0.0272	0.31077 0.0576	0.30906 0.0590	0.23523 0.1551	0.33924 0.0372
BLength	0.74368 <.0001	0.40302 0.0121	0.01607 0.9237	1.00000	0.05647 0.7363	0.06283 0.7078	0.01563 0.9258	0.08195 0.6248	0.09850 0.5563
Av1	0.18567 0.2644	0.43608 0.0062	0.35826 0.0272	0.05647 0.7363	1.00000	0.86219 <.0001	0.83012 <.0001	0.90129 <.0001	0.96307 <.0001
Av2	0.10639 0.5249	0.34689 0.0330	0.31077 0.0576	0.06283 0.7078	0.86219 <.0001	1.00000	0.97368 <.0001	0.92233 <.0001	0.83454 <.0001
Av3	0.05456 0.7449	0.32018 0.0500	0.30906 0.0590	0.01563 0.9258	0.83012 <.0001	0.97368 <.0001	1.00000	0.93448 <.0001	0.80905 <.0001
Av4	0.15872 0.3412	0.31207 0.0565	0.23523 0.1551	0.08195 0.6248	0.90129 <.0001	0.92233 <.0001	0.93448 <.0001	1.00000	0.91684 <.0001
Av5	0.20823 0.2096	0.43637 0.0062	0.33924 0.0372	0.09850 0.5563	0.96307 <.0001	0.83454 <.0001	0.80905 <.0001	0.91684 <.0001	1.00000

Figure B5: Density data analysis from SAS for combined population.

Appendix C: Results from Previous Studies

Table C1: Details of Existing Sizes of Headless Screws.

Company	Screw Name	Indications	Thread Design	Material	Shaft Diameter, mm	Major Thread Diameter at Tip, mm	Major Thread Diameter at Head, mm
AcuMed	Acutrak Mini	Radial head, capitellum, metacarpal, IP arthrodesis	Full, variable pitch	Ti	Tapered	2.8	3.1–3.6
AcuMed	Acutrak 2 Micro	Radial head, capitellum, metacarpal, IP arthrodesis	Full, variable pitch	Ti	Tapered	2.5	2.8
Arthrex	Micro Compression FT	Radial head, IP arthrodesis, metacarpal	Full, stepped variable pitch	Ti	Tapered	2.8	2.8
Integra	BOLD 2.5	Radial head, IP arthrodesis, metacarpal	Dual, partial variable pitch	Ti	1.8	2.5	3.3
KLS Martin	2.5 HBS 2 Mini∗	Radial head, capitellum, metacarpal, IP arthrodesis	Dual, variable pitch	Ti	1.7	2.5	3.2
Medartis	2.2 SpeedTip CCS	DIP arthrodesis, metacarpal	Dual, variable pitch	Ti	1.7	2.2	2.8
OsteoMed	2.0 HCS Extremifix	DIP arthrodesis, metacarpal	Dual, variable pitch	Ti	1.8	2.1	2.7

Table C1 (continued)

Company	Screw Name	Indications	Thread Design	Material	Shaft Diameter, mm	Major Thread Diameter at Tip, mm	Major Thread Diameter at Head, mm
OsteoMed	2.4 HCS Extremifix	Radial head, capitellum, metacarpal, IP arthrodesis	Dual, variable pitch	Ti	1.9	2.46	2.9
Small Bone Innovations	AutoFIX 2.0	DIP arthrodesis, metacarpal	Dual, variable pitch	SS	1.6	2	3
Small Bone Innovations	AutoFIX 2.5	Radial head, capitellum, metacarpal, IP arthrodesis	Dual, variable pitch	SS	1.8	2.5	3.3
Synthes	HCS 1.5	DIP arthrodesis, phalanx, metacarpal	Dual, non-variable pitch	SS, Ti	1.2	1.5	2.2
Synthes	HCS 2.4	Radial head, capitellum, metacarpal, IP arthrodesis	Dual, non-variable pitch	SS, Ti	2	2.4	3.1
TriMed	1.7 Small Headless Screw	DIP arthrodesis, phalanx, metacarpal	Dual, variable pitch	Ti	1.27	1.7	2.8
Zimmer	Herbert Mini Bone Screw	Metacarpal, carpal, IP arthrodesis	Dual, variable pitch	Ti	1.25	2.5	3.2

Table C2: Details of Existing Sizes of Headed Cannulated Screws.

Company	Screw	Thread Design	Material	Shaft Diameter, mm	Major Thread Diameter at Tip, mm	Guide Wire, mm	Length (Step Increment), mm
OsteoMed	2.0 Extremifix	Partial threads	Ti	1.8	2.1	0.9	6–42 (2)
OsteoMed	2.4 Extremifix	Partial threads	Ti	1.9	2.5	0.9	6–50 (2)
OsteoMed	3.0 Extremifix	Partial threads	Ti	2.2	3	1.1	10–40 (2)
Smith and Nephew	2.5 cannulated	Partial	SS	1.8	2.5	0.9	8–20 (1), 22–40 (2)
Smith and Nephew	3.0 cannulated	Partial	SS	2	3	1.1	8–20 (1), 22–40 (2)
Stryker	Asnis micro 2.0	Partial	Ti	1.7	2.1	0.8	8–20 (1), 22–30 (2)
Stryker	Asnis micro 3.0	Partial	Ti	2.1	3.1	1.2	8–30 (1), 32–40 (2)
Synthes	2.4 cannulated	Partial thread, short or long	SS	1.7	2.4	0.8	17–20 (1), 22–30 (2)
Synthes	2.4 cannulated	Partial thread, short or long	Ti	1.9	2.4	0.8	17–20 (1), 22–30 (2)
Synthes	3.0 cannulated	Partial thread, short or long	B	2	3	1.1	8–30 (1), 32–40 (2)
Synthes	3.5 cannulated	Partial or full	B	2.4	3.5	1.3	10–50 (2)
Arthrex	2.0 QuickFix cannulated	Partial	Ti	1.7	2	0.9	8–30 (2)
Arthrex	2.4 QuickFix cannulated	Partial	Ti	1.7	2.4	0.9	8–36 (2)
Arthrex	3.0 QuickFix cannulated	Partial	Ti	2	3	1.1	10–50 (2)

Table C3: Results from the Study of Michael Rivlin et al.

Averaged measurements	Fifth Metacarpal		Fourth metacarpal	
	(mm)	SD	(mm)	SD
Metacarpal length	89	21	95	22
Proximal third diameter (lateral)	13	4	14	5
Distal third diameter (lateral)	16	4	16	4
Proximal third diameter (AP)	16	5	14	4
Distal third diameter (AP)	16	5	16	5
	(deg)	SD	(deg)	SD
Shaft bending angle (lateral)	10	3	12	3
Capital-axis angle (lateral)	12	6	14	12
Shaft bending angle (AP)	1	2	0	1
Radius of curvature (lateral)	256 mm		228 mm	

Appendix D: Table of Terminology

Table D1: Table of Terminology Used in the Methodology of Chapter 3.

N	Number of voxels included for volumetric model
(xi, yi, zi)	Coordinates of the volumetric model
[Gx, Gy, Gz]	Global coordinate system
[Lx, Ly, Lz]	Local coordinate system
[Cx, Cy, Cz]	Geometric center of the bone
P1	Eigen vector for first principal component
P2	Eigen vector for second principal component
P3	Eigen vector for third principal component
CIC	Canal inscribed circle
CCC	Canal circumscribed circle
OIC	Outer inscribed circle
OCC	Outer circumscribed circle
Thick1	Diam OIC- Diam CCC

Appendix E: Copyright Permissions

1) Copyright permission for tables C1 and C2 was obtained as below:

ELSEVIER LICENSE
TERMS AND CONDITIONS
Oct 29, 2019

This Agreement between University of South Florida ("You") and Elsevier ("Elsevier") consists of your license details and the terms and conditions provided by Elsevier and Copyright Clearance Center.

License Number	4698370357026
License date	Oct 29, 2019
Licensed Content Publisher	Elsevier
Licensed Content Publication	The Journal of Hand Surgery
Licensed Content Title	Nuts and Bolts: Dimensions of Commonly Utilized Screws in Upper Extremity Surgery
Licensed Content Author	Nathan Douglass, Jeffrey Yao
Licensed Content Date	Feb 1, 2015
Licensed Content Volume	40
Licensed Content Issue	2
Licensed Content Pages	15
Start Page	368
End Page	382
Type of Use	reuse in a thesis/dissertation
Portion	figures/tables/illustrations
Number of figures/tables/illustrations	2
Format	electronic
Are you the author of this Elsevier article?	No
Will you be translating?	No
Title	Morphometry and Density Analysis of the Fifth Metacarpal
Institution name	University of South Florida
Expected presentation date	Oct 2019
Portions	Table 1 & 2

Figure E1: Permission from Elsevier for the tables on screw sizes.

	University of South Florida 4120, Ashford Green Apartments, J 102
Requestor Location	TAMPA, FL 33613 United States Attn: University of South Florida
Publisher Tax ID	98-0397604
Total	0.00 USD

Terms and Conditions

INTRODUCTION

1. The publisher for this copyrighted material is Elsevier. By clicking "accept" in connection with completing this licensing transaction, you agree that the following terms and conditions apply to this transaction (along with the Billing and Payment terms and conditions established by Copyright Clearance Center, Inc. ("CCC"), at the time that you opened your Rightslink account and that are available at any time at http://myaccount.copyright.com).

GENERAL TERMS

2. Elsevier hereby grants you permission to reproduce the aforementioned material subject to the terms and conditions indicated.

3. Acknowledgement: If any part of the material to be used (for example, figures) has appeared in our publication with credit or acknowledgement to another source, permission must also be sought from that source. If such permission is not obtained then that material may not be included in your publication/copies. Suitable acknowledgement to the source must be made, either as a footnote or in a reference list at the end of your publication, as follows:

"Reprinted from Publication title, Vol /edition number, Author(s), Title of article / title of chapter, Pages No., Copyright (Year), with permission from Elsevier [OR APPLICABLE SOCIETY COPYRIGHT OWNER]." Also Lancet special credit - "Reprinted from The Lancet, Vol. number, Author(s), Title of article, Pages No., Copyright (Year), with permission from Elsevier."

4. Reproduction of this material is confined to the purpose and/or media for which permission is hereby given.

Figure E1 (continued)

5. Altering/Modifying Material: Not Permitted. However figures and illustrations may be altered/adapted minimally to serve your work. Any other abbreviations, additions, deletions and/or any other alterations shall be made only with prior written authorization of Elsevier Ltd. (Please contact Elsevier at permissions@elsevier.com). No modifications can be made to any Lancet figures/tables and they must be reproduced in full.

6. If the permission fee for the requested use of our material is waived in this instance, please be advised that your future requests for Elsevier materials may attract a fee.

7. Reservation of Rights: Publisher reserves all rights not specifically granted in the combination of (i) the license details provided by you and accepted in the course of this licensing transaction, (ii) these terms and conditions and (iii) CCC's Billing and Payment terms and conditions.

8. License Contingent Upon Payment: While you may exercise the rights licensed immediately upon issuance of the license at the end of the licensing process for the transaction, provided that you have disclosed complete and accurate details of your proposed use, no license is finally effective unless and until full payment is received from you (either by publisher or by CCC) as provided in CCC's Billing and Payment terms and conditions. If full payment is not received on a timely basis, then any license preliminarily granted shall be deemed automatically revoked and shall be void as if never granted. Further, in the event that you breach any of these terms and conditions or any of CCC's Billing and Payment terms and conditions, the license is automatically revoked and shall be void as if never granted. Use of materials as described in a revoked license, as well as any use of the materials beyond the scope of an unrevoked license, may constitute copyright infringement and publisher reserves the right to take any and all action to protect its copyright in the materials.

9. Warranties: Publisher makes no representations or warranties with respect to the licensed material.

10. Indemnity: You hereby indemnify and agree to hold harmless publisher and CCC, and their respective officers, directors, employees and agents, from and against any and all claims arising out of your use of the licensed material other than as specifically authorized pursuant to this license.

Figure E1 (continued)

11. No Transfer of License: This license is personal to you and may not be sublicensed, assigned, or transferred by you to any other person without publisher's written permission.

12. No Amendment Except in Writing: This license may not be amended except in a writing signed by both parties (or, in the case of publisher, by CCC on publisher's behalf).

13. Objection to Contrary Terms: Publisher hereby objects to any terms contained in any purchase order, acknowledgment, check endorsement or other writing prepared by you, which terms are inconsistent with these terms and conditions or CCC's Billing and Payment terms and conditions. These terms and conditions, together with CCC's Billing and Payment terms and conditions (which are incorporated herein), comprise the entire agreement between you and publisher (and CCC) concerning this licensing transaction. In the event of any conflict between your obligations established by these terms and conditions and those established by CCC's Billing and Payment terms and conditions, these terms and conditions shall control.

14. Revocation: Elsevier or Copyright Clearance Center may deny the permissions described in this License at their sole discretion, for any reason or no reason, with a full refund payable to you. Notice of such denial will be made using the contact information provided by you. Failure to receive such notice will not alter or invalidate the denial. In no event will Elsevier or Copyright Clearance Center be responsible or liable for any costs, expenses or damage incurred by you as a result of a denial of your permission request, other than a refund of the amount(s) paid by you to Elsevier and/or Copyright Clearance Center for denied permissions.

LIMITED LICENSE

The following terms and conditions apply only to specific license types:

15. **Translation**: This permission is granted for non-exclusive world **English** rights only unless your license was granted for translation rights. If you licensed translation rights you may only translate this content into the languages you requested. A professional translator must perform all translations and reproduce the content word for word preserving the integrity of the article.

16. **Posting licensed content on any Website**: The following terms and conditions apply as follows: Licensing material from an Elsevier journal: All content posted to the web site must maintain the copyright information line on

Figure E1 (continued)

the bottom of each image; A hyper-text must be included to the Homepage of the journal from which you are licensing at http://www.sciencedirect.com/science/journal/xxxxx or the Elsevier homepage for books at http://www.elsevier.com; Central Storage: This license does not include permission for a scanned version of the material to be stored in a central repository such as that provided by Heron/XanEdu.

Licensing material from an Elsevier book: A hyper-text link must be included to the Elsevier homepage at http://www.elsevier.com . All content posted to the web site must maintain the copyright information line on the bottom of each image.

Posting licensed content on Electronic reserve: In addition to the above the following clauses are applicable: The web site must be password-protected and made available only to bona fide students registered on a relevant course. This permission is granted for 1 year only. You may obtain a new license for future website posting.

17. **For journal authors**: the following clauses are applicable in addition to the above:

Preprints:

A preprint is an author's own write-up of research results and analysis, it has not been peer-reviewed, nor has it had any other value added to it by a publisher (such as formatting, copyright, technical enhancement etc.).

Authors can share their preprints anywhere at any time. Preprints should not be added to or enhanced in any way in order to appear more like, or to substitute for, the final versions of articles however authors can update their preprints on arXiv or RePEc with their Accepted Author Manuscript (see below).

If accepted for publication, we encourage authors to link from the preprint to their formal publication via its DOI. Millions of researchers have access to the formal publications on ScienceDirect, and so links will help users to find, access, cite and use the best available version. Please note that Cell Press, The Lancet and some society-owned have different preprint policies. Information on these policies is available on the journal homepage.

Accepted Author Manuscripts: An accepted author manuscript is the manuscript of an article that has been accepted for publication and which

Figure E1 (continued)

typically includes author-incorporated changes suggested during submission, peer review and editor-author communications.

Authors can share their accepted author manuscript:

- immediately
  - via their non-commercial person homepage or blog
  - by updating a preprint in arXiv or RePEc with the accepted manuscript
  - via their research institute or institutional repository for internal institutional uses or as part of an invitation-only research collaboration work-group
  - directly by providing copies to their students or to research collaborators for their personal use
  - for private scholarly sharing as part of an invitation-only work group on commercial sites with which Elsevier has an agreement
- After the embargo period
  - via non-commercial hosting platforms such as their institutional repository
  - via commercial sites with which Elsevier has an agreement

In all cases accepted manuscripts should:

- link to the formal publication via its DOI
- bear a CC-BY-NC-ND license - this is easy to do
- if aggregated with other manuscripts, for example in a repository or other site, be shared in alignment with our hosting policy not be added to or enhanced in any way to appear more like, or to substitute for, the published journal article.

Published journal article (JPA): A published journal article (PJA) is the definitive final record of published research that appears or will appear in the journal and embodies all value-adding publishing activities including peer review co-ordination, copy-editing, formatting, (if relevant) pagination and online enrichment.

Policies for sharing publishing journal articles differ for subscription and gold open access articles:

Subscription Articles: If you are an author, please share a link to your article rather than the full-text. Millions of researchers have access to the formal

Figure E1 (continued)

publications on ScienceDirect, and so links will help your users to find, access, cite, and use the best available version.

Theses and dissertations which contain embedded PJAs as part of the formal submission can be posted publicly by the awarding institution with DOI links back to the formal publications on ScienceDirect.

If you are affiliated with a library that subscribes to ScienceDirect you have additional private sharing rights for others' research accessed under that agreement. This includes use for classroom teaching and internal training at the institution (including use in course packs and courseware programs), and inclusion of the article for grant funding purposes.

Gold Open Access Articles: May be shared according to the author-selected end-user license and should contain a CrossMark logo, the end user license, and a DOI link to the formal publication on ScienceDirect.

Please refer to Elsevier's posting policy for further information.

18. **For book authors** the following clauses are applicable in addition to the above: Authors are permitted to place a brief summary of their work online only. You are not allowed to download and post the published electronic version of your chapter, nor may you scan the printed edition to create an electronic version. **Posting to a repository**: Authors are permitted to post a summary of their chapter only in their institution's repository.

19. **Thesis/Dissertation**: If your license is for use in a thesis/dissertation your thesis may be submitted to your institution in either print or electronic form. Should your thesis be published commercially, please reapply for permission. These requirements include permission for the Library and Archives of Canada to supply single copies, on demand, of the complete thesis and include permission for Proquest/UMI to supply single copies, on demand, of the complete thesis. Should your thesis be published commercially, please reapply for permission. Theses and dissertations which contain embedded PJAs as part of the formal submission can be posted publicly by the awarding institution with DOI links back to the formal publications on ScienceDirect.

Figure E1 (continued)

Elsevier Open Access Terms and Conditions

You can publish open access with Elsevier in hundreds of open access journals or in nearly 2000 established subscription journals that support open access publishing. Permitted third party re-use of these open access articles is defined by the author's choice of Creative Commons user license. See our open access license policy for more information.

Terms & Conditions applicable to all Open Access articles published with Elsevier:

Any reuse of the article must not represent the author as endorsing the adaptation of the article nor should the article be modified in such a way as to damage the author's honour or reputation. If any changes have been made, such changes must be clearly indicated.

The author(s) must be appropriately credited and we ask that you include the end user license and a DOI link to the formal publication on ScienceDirect.

If any part of the material to be used (for example, figures) has appeared in our publication with credit or acknowledgement to another source it is the responsibility of the user to ensure their reuse complies with the terms and conditions determined by the rights holder.

Additional Terms & Conditions applicable to each Creative Commons user license:

CC BY: The CC-BY license allows users to copy, to create extracts, abstracts and new works from the Article, to alter and revise the Article and to make commercial use of the Article (including reuse and/or resale of the Article by commercial entities), provided the user gives appropriate credit (with a link to the formal publication through the relevant DOI), provides a link to the license, indicates if changes were made and the licensor is not represented as endorsing the use made of the work. The full details of the license are available at http://creativecommons.org/licenses/by/4.0.

CC BY NC SA: The CC BY-NC-SA license allows users to copy, to create extracts, abstracts and new works from the Article, to alter and revise the Article, provided this is not done for commercial purposes, and that the user gives appropriate credit (with a link to the formal publication through the relevant DOI), provides a link to the license, indicates if changes were made and the licensor is not represented as endorsing the use made of the work. Further, any

Figure E1 (continued)

new works must be made available on the same conditions. The full details of the license are available at http://creativecommons.org/licenses/by-nc-sa/4.0.

CC BY NC ND: The CC BY-NC-ND license allows users to copy and distribute the Article, provided this is not done for commercial purposes and further does not permit distribution of the Article if it is changed or edited in any way, and provided the user gives appropriate credit (with a link to the formal publication through the relevant DOI), provides a link to the license, and that the licensor is not represented as endorsing the use made of the work. The full details of the license are available at http://creativecommons.org/licenses/by-nc-nd/4.0. Any commercial reuse of Open Access articles published with a CC BY NC SA or CC BY NC ND license requires permission from Elsevier and will be subject to a fee.

Commercial reuse includes:

- Associating advertising with the full text of the Article
- Charging fees for document delivery or access
- Article aggregation
- Systematic distribution via e-mail lists or share buttons

Posting or linking by commercial companies for use by customers of those companies.

20. **Other Conditions**:

v1.9

Questions? customercare@copyright.com or +1-855-239-3415 (toll free in the US) or +1-978-646-2777.

Figure E1 (continued)

2) The copyright permission for table C3 was obtained as below:

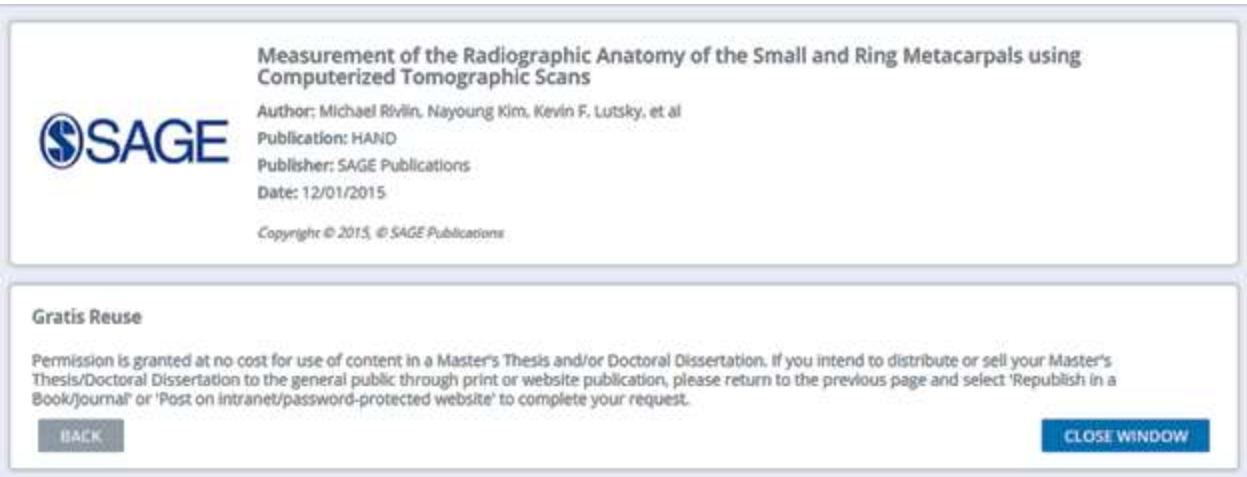

Figure E2: Copyright permission from SAGE publications.